Identifying the Antarctic melt contribution to Last Interglacial sea level from Eurasian relative sea-level records

Oliver G. Pollard[1], Natasha L.M. Barlow[1], Lauren J. Gregoire[1], Natalya Gomez[2], Lachlan C. Astfalck[3], Amy M. McGuire[1]

1 School of Earth and Environment, University of Leeds, Leeds, UK
2 Department of Earth and Planetary Sciences, McGill University, Montreal, QC, Canada
3 School of Physics, Mathematics & Computing, The University of Western Australia, Crawley, Australia

* o.g.pollard@leeds.ac.uk

Abstract

High global mean sea level during the Last Interglacial (LIG) was likely to have largely been driven by Greenland and Antarctic melt, but the timings, rates, and relative magnitudes of these contributions remain elusive. Due to the geometry of ice-sheet fingerprints, relative sea level records in the Eurasian region are likely to be sensitive to ice mass changes in Antarctica while being relatively insensitive to changes in Greenland, making them ideal targets for identifying scenarios of past Last Interglacial ice-sheet melt. We produce an ensemble of Eurasian relative sea level models, driven by regional glacial-isostatic adjustment due to the penultimate glacial cycle, and a systematic suite of Antarctic melt scenarios in order to compare our simulations against Last Interglacial relative sea level records from the WALIS sea level database. By performing regional sensitivity analysis, we identify Eurasian data regions most sensitive to Antarctic ice sheet melt. Through the use of a bespoke Bayesian history matching framework, we uncover glacial isostatic adjustment and Antarctic ice sheet melt scenarios that most closely match regional relative sea level data within uncertainty. Our results show that data points off the coast of Wales, northwest France, and the English Channel are most sensitive to Antarctic melt but that all modelled relative sea level scenarios are able to fit the suite of relative sea level data within 3-sigma uncertainty. Despite this, by utilising relative sea level data that we have identified as strongly sensitive to Antarctic ice-sheet changes, our data-model analysis reveals a clear preference for high magnitudes of total melt, identifying an Antarctic contribution of between 3.2 - 9.3 m to the Last Interglacial global mean sea level highstand (*likely*, 66th percentile).

Author summary

Sea level is rising as the climate warms, but it remains difficult to determine how much of this rise will result from melting of the Antarctic Ice Sheet. The Last Interglacial, about 130,000 to 116,000 years ago, was a recent warm period when sea level was higher than today. Geological sea-level records from northwest Eurasia can help us understand past Antarctic ice loss because this region is more sensitive to Antarctic melting than to melting in Greenland. We combined these records with hundreds of computer simulations that represent uncertainty in the Earth's structure, former Eurasian ice

sheets, and the timing and size of Antarctic ice loss. Records from Wales, northwest France, and the English Channel were the most informative. Although current data and model uncertainty cannot exclude individual scenarios, the best-matching simulations favour substantial Antarctic melting: 3.2–9.3 m of global mean sea-level rise during the Last Interglacial. Better-dated sea-level records from these sensitive regions could provide stronger constraints on future Antarctic ice-sheet change.

Introduction

Modern anthropogenic activity is driving wide-scale sustained warming of Earth's climate and, in response, global mean sea level (GMSL) is projected to rise by upwards of 5 m under high emission scenarios by 2300 [1]. Despite this, our understanding of the response of modern-day ice sheets to future warming remains highly uncertain, particularly beyond 2300, primarily as a consequence of the need for numerical models to simulate ice-sheet behaviour outside of the window of modern observations [2,3]. The Earth system has been subjected to similar warming events during previous Quaternary interglacial periods and, of these events, the LIG (Marine Isotope Stage (MIS) 5e; c. 130-116 ka) represents the most recent, well-studied and data-rich past interglacial in which the Greenland Ice Sheet (GrIS) and Antarctic Ice Sheet (AIS) were thought to be smaller than those of today [4,5]. Constraining the evolution of the GrIS and AIS during the LIG would help to elucidate the sensitivity and response of these ice sheets to future warming.

There is wide agreement that GMSL during the LIG was higher than today, but studies differ in their estimates of its magnitude, varying between 1.2 m and 10 m above the current values, with even higher values not currently ruled out [6–9]. The contribution of thermal expansion to the LIG sea-level highstand has been constrained to $0.4 - 0.8$ m [10,11] while melt from mountain glaciers may have contributed up to 0.32 ± 0.08 m SLE [12] meaning that higher LIG sea levels cannot be explained without large contributions from the GrIS and/or AIS, or potentially the presence of ice over North America late in the interglacial [13]. Dynamic ice-sheet models driven by climate forcing assumed to be representative of the LIG, have been applied to the GrIS resulting in wide-ranging estimates of its LIG GMSL contribution of between 0.6 m SLE [14] and 5.3 m SLE [15], depending on the climate forcing, ice-sheet model, and proxy data constraints employed in the experimental design [14–16]. These estimates are of similar magnitude to those inferred from recent data studies that place GrIS between 0.6 - 3.5 m SLE [7]. AIS modelling studies have placed emphasis on identifying the distinct behaviour and drivers of the East Antarctic Ice Sheet (EAIS) and West Antarctic Ice Sheet (WAIS) melt. Coupled, dynamic ice-sheet simulations of the marine-based WAIS have suggested a LIG GMSL contribution of 1 - 5 m [17–19], driven primarily by the ice sheet's vulnerability to Southern Ocean warming [11], but these estimates may be under predicted by up to 30% if water expulsion from post-glacial rebound is accounted for [20]. The majority of the EAIS is relatively insensitive to ocean forcing, as most of the ice sheet sits on bedrock that lies above the sea-surface elevation, and has therefore been assumed to be relatively stable [21,22]. However, modelling by Fogwill et al. [23] found that the EAIS may be vulnerable to changes in Southern-Hemispheric wind patterns and the resulting local surface warming, driving 3 - 5 m LIG SLE contribution. AIS Penultimate Deglaciation to LIG melt scenarios in the study by Bradley et al. [24], in which such scenarios were evaluated against ice-core derived evidence of ice thickness, estimated that the majority of EAIS change occurs prior to 126 ka and found no more than a 1.1 m SLE LIG contribution from the EAIS using their reference ice-sheet model, while their adapted idealised Wilkes and Aurora basins retreat scenario contributed 1 m SLE.

Through the combined effects of Earth rotation, viscoelestic deformation and gravitational affects, the particular location and geometry of ice-sheet melt results in a distinct spatial pattern of relative sea level (RSL) (sometimes termed 'sea-level fingerprint') that, in turn, result in large differences in regional sensitivity to LIG AIS melt [13,25,26]. Efforts have been made to derive estimates of LIG AIS melt from records of RSL, in regions targeted for their high sensitivity to AIS changes, through the use of statistical methods [27,28]. Such work relies on well-constrained chronologies, quantified contributions of local processes, and assumptions about the contribution of the GrIS and, as a result, studies typically focus on a single region or record, for example, Barnett et al. [27] utilised a database of 27 absolute-dated LIG data points (7 limiting, 20 sea-level index points), primarily located in the English Channel region, corrected for regional glacial isostatic adjustment (GIA) and processes driving vertical land motion, to produce a single time series for regional LIG sea-level change. By subtracting an estimate for the GrIS contribution, the remaining time series was attributed to AIS melt and, using an estimate of the magnitude of the northwest Eurasia AIS fingerprint, was converted into an estimate for LIG AIS contribution of 5.7 m (median, 50th percentile), with a range of 3.6 to 8.7 m (central 68% probability). In other work, Dutton et al. [7] estimate a LIG AIS contribution of 4.6 ± 1.7 m by subtracting estimated GrIS, thermosteric, and mountain glacier contributions from the sea-level signal recorded by LIG corals in the Seychelles. Significant uncertainties remain in the rate, timing and magnitudes of LIG AIS melt, as well as in the relative contributions of WAIS and EAIS, and yet these constraints are vital for realising the potential of the LIG as a rich archive of empirical ocean, ice, and climate constraints for the calibrations of climate and ice sheet models used in future projections that inform present-day decision-making and policy [29, 30].

With the goal of better constraining the evolution of the LIG AIS, we develop a new data-model comparison framework that considers the underlying uncertainties in the LIG RSL datasets [31], the ice-sheet histories during LIG and the preceding glacial period [13, 28, 32] and the rheological model which underpins the solid Earth response to changes in ice load over time [26, 33]. Consideration of these combined uncertainties are not typically account for in published research to-date. We use a statistical uncertainty quantification procedure to identify the most plausible LIG AIS melt scenarios when compared against northwest Eurasian LIG RSL data. We ran a large ensemble of gravitationally self-consistent sea-level model simulations that span uncertainties in AIS evolution during the LIG, Eurasian ice sheet penultimate deglaciation, and solid earth structure and compared them against an extensive, newly compiled Eurasian LIG RSL database. Sensitivity analysis of our ensemble enables us to determine the relative sensitivity of northwest Eurasian regions to AIS melt and our "history matching" uncertainty quantification procedure allowed us to identify regions of our parameter space that best match northwest Eurasian records of RSL. Finally, we combine information gained from this analysis to identify the most likely scenarios of LIG AIS evolution.

Models, methods and data

Using a gravitationally self-consistent sea-level model [34], we simulated LIG RSL constructing an ensemble of possible input AIS melt histories spanning a range of timings, durations, and volumes. We ran an ensemble of sea level simulations that efficiently spanned the range of uncertainties in AIS melt histories, Earth model parameters, global ice sheet histories and the Eurasian penultimate deglaciation. The resulting model outputs were then evaluated against a European RSL database [31] using an implausibility metric that accounts for uncertainty in the amplitude and timing of the data and accounts for model biases.

Global ice-sheet and Earth structure models

We use the gravitationally self-consistent sea-level model described in Han et al. [34] which follows the theory and algorithm described in [35]. The model takes global ice-sheet thickness changes and a 1D model of viscoelastic Earth structure as input in order to generate solutions to the Sea Level Equation, accounting for the effects of gravitation, Earth rotation and viscoelastic deformation of the solid Earth and shoreline migration including migration of water into areas freed of marine based ice [36, 37]. Sea-level model calculations are performed using a pseudo-spectral algorithm up spherical harmonic degree 512 and, as a result, model RSL and topography outputs, as well as ice-sheet history inputs, are provided on a 512 by 1024 Gauss–Legendre latitude-longitude grid (hereafter referred to as the model grid). The Earth model assumes an elastically compressible 1D Maxwell structure with a radially varying, stepped viscosity profile which is parameterised by an upper-mantle viscosity ν_{UM}, lower mantle viscosity ν_{LM}, and lithospheric thickness L and which preserves the location of Preliminary Reference Earth Model (PREM) discontinuities. As demonstrated by Pollard et al. [33], the Earth model uncertainty is a dominant contributor to LIG RSL uncertainty in our study area and therefore, we include systematic exploration of the viscoelastic Earth structure in our experimental design. We adopt the Earth model parameter ranges developed for the northwest European region by Bradley et al. [38] of 0.1 - 1 $\times 10^{21}$ Pa s for ν_{UM}, $0.1 - 5 \times 10^{22}$ Pa s for ν_{LM} and $71 - 96 \times 10^3$ km for L, based upon regional published literature [38–40].

Interglacial RSL values are sensitive to ice-sheet changes from at least 3 glacial cycles prior to the interglacial period of interest, as shown by Dendy et al. [39], while the sea-level model requires the ice-sheet history to extend to modern-day to enable convergence to modern topography. Therefore, we prescribe global ice-sheet changes from 420 ka until the modern day by scaling the Peltier et al. [41] ICE-6G global ice-sheet model of the Last Glacial Period to a global ice-sheet volume curve derived from the δ^{18}O reconstruction of Waelbroeck et al. [42]. Since the Penultimate Glacial Period ice-sheet configuration in North America and Eurasia was likely very different to that of the Last Glacial Period we modify the Penultimate Glacial Period section of our ice history by replacing the Eurasian ice-sheet with an ensemble of deglaciation geometries, as outlined in Pollard et al. [33], and re-scale the North American ice-sheet in order to match the total global ice-sheet budget at the Penultimate Glacial Maximum (PGM). Our previous study demonstrated that LIG RSL in Eurasia is relatively insensitive to the timing of North American and Eurasian deglaciation [33] and so we prescribe a fixed PGM timing for both the Eurasian and North American ice sheets of 139 ka and also terminate their deglaciations at 129 ka. During the LIG portion of our ice-sheet history (between 129 ka and 116 ka) we only vary AIS melt between ensemble members. We prescribe a set melt scenario for the /acgris while setting all other ice sheets to their static, pre-industrial configurations.

Last Interglacial Antarctic melt scenarios

We construct a range of LIG AIS melt scenarios that differ in the rate, timing, and magnitude of both WAIS and EAIS melt contributions. To generate our scenarios, we consider the evolution of WAIS and EAIS separately. We generate time series of ice volume change for each ice sheet during the LIG (that prescribe when ice is lost/gained) which are then converted into corresponding AIS ice-thickness changes by interpolating a series of pre-modelled AIS thickness configurations (henceforth termed 'the base model').

Our base model is the Representative Concentration Pathway (RCP) 8.5 high emission, marine ice cliff instability (MICI) inclusive scenario of Deconto et al. [30], chosen as it spans a large range of AIS volumes, maximising the range of melt scenarios we are able to test. The model consists of 56 model time-steps spanning from the modern-day (pre-industrial) AIS configuration until 2500, which we interpolate onto the same lat-long model grid as used in our study. To prepare this model for use in our interpolation methodology, we first split the DeConto model into separate EAIS and WAIS ice-thickness series with the boundary between the two given by the MEaSUREs Antarctic Boundaries dataset [43], before then calculating the volume of grounded ice for each region and model time step. The 56 ice-thickness configurations for EAIS and WAIS are then tied to an ice-sheet volume rather than a time step so that their ice-thickness values can be interpolated between with respect to ice-sheet volume. In its modern configuration and topography, the Deconto et al. [30] model simulation contains 5.6 m SLE and 50.2 m SLE grounded ice volume for WAIS and EAIS respectively and, in its minimum configuration, this reduces to 1.6 m SLE for WAIS and 42.9 m SLE for EAIS. The regionally divided ice-sheet model combined with calculated grounded ice-sheet volumes allows for interpolating ice configurations that correspond to any prescribed value of grounded ice volume and, by extension, melt contribution.

We parameterise the LIG AIS melt scenarios (Fig 1) with one set of parameters controlling the evolution of WAIS volume and another set of parameters controlling the EAIS. We describe WAIS melt with four parameters: melt start time T^{WA}_{melt}, the time at which melting from the default, present-day configuration occurs; melt volume V^{WA}_{melt}, describing the maximum magnitude of melting; duration of melt d^{WA}_{melt}, determining how long the transition from present-day to maximum melt configuration takes; and the stability duration d^{WA}_{stable}, which determines how long WAIS will remain in the fully melted configuration before returning to modern at 116 ka. To avoid $T^{WA}_{melt} + d^{WA}_{melt} + d^{WA}_{stable} > 116$ ka, we determine d^{WA}_{stable} by the parameter p^{WA} controlling the percentage of the LIG after $T^{WA}_{melt} + d^{WA}_{melt}$ that should remain stable. After sampling, we convert values of p^{WA}_{stable} to d^{WA}_{stable} by,

$$d^{WA}_{stable} = p^{WA}_{stable}(T^{WA}_{melt} + D^{WA}_{melt} - 116). \tag{1}$$

The transition between the modern configuration, pre-melt state and the fully melted state follows a half cosine decay function (see example in Fig 1B) reflecting our assumption of a fast initial melting that decelerates towards V^{WA}_{melt}, as supported by Golledge et al. [19], while a linear transition is assumed between the end of d^{WA}_{stable} and the return to the modern state at 116 ka.

For the EAIS, we assume that changes in volume occurred more gradually and that the ice sheet likely never equilibrated. In addition, since evidence suggests the possibility EAIS growth under modern-day warming [44], we do not rule out the possibility of EAIS growth during the LIG. Therefore, we allow scenarios to include negative values of EAIS volume and, for clarity, refer to EAIS parameters as determining ice-sheet change rather than melt. We do not include a period of stability as we do for the WAIS, but otherwise similarly describe EAIS scenarios with three parameters: change start time T^{EA}_{change}, change volume V^{EA}_{change}, and duration of change d^{EA}_{change}. To reflect the assumption of a more gradual EAIS evolution, we use

Fig 1. Antarctic Melt Parameterisation. (A) The last interglacial is divided into periods of ice-sheet melt (blue), stability (yellow) and growth (red) and different parameters control East and West Antarctic ice sheets. For the EAIS, we parameterise the magnitude (V^{EA}_{melt}), duration (d^{EA}_{melt}) and initial time of melt (T^{EA}_{melt}). We define equivalent parameters for WAIS but with the addition of p^{WA}_{stable} which determines the percentage of the melt period (between T^{WA}_{melt} and 116 ka) for which WAIS remains in a stable, minimum volume configuration. (B) An illustrative example of an AIS melt scenario labelled with each parameter.

a low degree (N=1.3) polynomial transition function but keep the assumption of linear growth from V^{EA}_{change} back to the modern-day configuration at 116 ka. For scenarios that test EAIS ice-sheet growth, we require EAIS ice thickness configurations thicker than exist in the DeConto series and so, in this case, we uniformly scale the base model ice configuration to match the required volume.

For each member in our ensemble of volume time-series for EAIS and WAIS, we generated an AIS ice-sheet history based on the ice-sheet geometries of the modern-day DeConto model. To do so, we first calculated the grounded ice-sheet volume associated with each DeConto model time step when placed on LIG topography. We then discarded the temporal ordering of these ice-sheet geometries and re-ordered them to be monotonically increasing in terms of grounded ice-sheet volume. This allowed us to generate a new ice-sheet geometry of a given grounded-ice volume by linearly interpolating this series of volumes and then uniformly applying the same interpolant to the associated series of ice-sheet thickness pixels. The ensemble of Antarctic melt scenarios thus generated is shown in Fig 2.

We chose to use LIG topography, as opposed to the original modern-day topography, to avoid discrepancies in grounded ice-sheet volumes and therefore the total potential global mean sea-level contribution of each geometry. When compared, we found an absolute reduction of 0.4 m SLE and 0.3 m SLE for WAIS and EAIS volumes between modern and LIG topographies, respectively. The DeConto modern topography is temporally variable, while our LIG topography was not. However, we found a near-linear relationship between the modern-day and LIG V^{EA}_{change} (gradient 0.97) and V^{WA}_{melt} (gradient 0.94) topography-derived volume values, demonstrating negligible impact of these temporal changes on the total grounded ice-sheet volume.

Table 1. Antarctic melt scenario parameters and their corresponding ranges.

Name	Symbol	Range	Unit
WAIS Melt Start Time	T^{WA}_{melt}	129 - 124	ka
WAIS Melt Duration	d^{WA}_{melt}	0.5 - 3	ka
WAIS Melt Volume	V^{WA}_{melt}	0 - 5.5	m SLE
WAIS Stability Percentage	p^{WA}_{stable}	0.2 - 0.8	1
EAIS Change Start Time	T^{EA}_{change}	129 - 124	ka
EAIS Change Duration	d^{EA}_{change}	1 - 9	ka
EAIS Volume Change	V^{EA}_{change}	-1 - 5	m SLE

Relative sea-level ensemble design

In addition to the 7 parameters controlling the evolution of LIG Antarctic melt (Table 1), our ensemble design consists of 3 parameters describing the viscoelastic Earth model and 3 derived parameters describing the regional ice-sheet volume of the Eurasian ice-sheet during the Penultimate Deglaciation (Table 2). Pollard et al. [33] demonstrated that the Eurasian ice-sheet volume was, in some Eurasian regions, the dominant contributor to uncertainty in LIG RSL. To account for this source of uncertainty, we design our ensemble to use the suite of 532 Eurasian deglaciation geometries as generated by Pollard et al. [33]. Alongside, we generate a 532-member latin hypercube sample (LHS) of our 3 Earth model parameters (Table

1) and 7 AIS history parameters assuming a uniform distribution across parameter ranges (Table 2) resulting in 532 Earth models and LIG Antarctic melt scenarios to test. We run the resulting set of 532 global ice-sheet histories and Earth model configurations with the sea-level model to produce an ensemble of RSL simulations spanning from 420 ka until the present day.

Table 2. Relative Sea-Level Ensemble Parameters. Earth model and Eurasian ice-sheet model parameters varied in our ensemble of simulations. Probability distributions used for the sampling are noted as $U(min, max)$ for a uniform distribution between min and max or $N(\mu, \sigma)$ for a normal distribution with mean μ and standard deviation σ.

Name	Symbol	Distribution	Unit
Upper Mantle Viscosity	ν_{UM}	$U(0.1, 1) \times 10^{21}$	Pa s
Lower Mantle Viscosity	ν_{LM}	$U(0.1, 5) \times 10^{22}$	Pa s
Lithospheric Thickness	L	$U(71, 96) \times 10^{3}$	km
Barents-Kara Sea Eurasian Ice-Sheet Volume	V_{BKS}^{Er}	$N(28, 4)$	m SLE
Fennoscandian Eurasian Ice-Sheet Volume	V_{F}^{Er}	$N(24, 3)$	m SLE
British-Irish Eurasian Ice-Sheet Volume	V_{BI}^{Er}	$N(1.8, 0.1)$	m SLE

Fig 2. Antarctica Ensemble. Ensemble of Antarctic melt scenarios generated with our parameterisation. (Top) WAIS, EAIS, and total AIS sea-level contributions during the LIG with ensemble 5th and 9th percentile (light shading), 32 and 68th percentile (dark shading), and median value (solid line). Individual ensemble members are shown as light grey lines. (Bottom) AIS ice-sheet thickness ensemble mean (blue) and standard deviation (purple) at 128, 124, 122, and 118 ka.

Last Interglacial sea-level database

Empirical observations of LIG RSL were sourced from World Atlas of Last Interglacial Shorelines (WALIS), a state-of-the-art LIG RSL database containing 6600 RSL data points [31]. Each RSL value, representing RSL at a specified location, can broadly be categorised as either a: sea-level index, representing a value that RSL attained; marine limiting, representing a value that RSL exceeded; and terrestrial limiting, which RSL remained below [45]. In addition, the age associated with each data point can be categorised as absolute, which provides a specific age value with uncertainty (e.g. an OSL date); or relative (or floating), whereby the data point may have occurred at any time within a time range determined by the chronological constraint to which it is tied to (e.g. pollen biostratigraphy). We initially filtered the WALIS dataset to only include data points: (i) at locations within the northwest Eurasian region (which comprises the regional compilations of Cohen et al. [46], and Dalton et al. [47]), (ii) with an age range overlapping with the timing of LIG (129 - 116 ka, [7]), and (iii) those data points that include a specified RSL uncertainty (see Fig 3). After this filtering, our dataset contains 93 sea-level index, 210 marine limiting, and 14 terrestrial limiting data points, of which 120 have absolute ages and 197 have relative ages, at 141 unique locations, as shown in Fig 4. Also shown in Fig 4 are the 13 regions used to group the data points for regional-specific analysis and comparison against the RSL ensemble.

Fig 3. Relative Sea-Level Data Filtering. Schematic of the filtering process applied to RSL data points.

RSL and associated uncertainty values from WALIS represent the observed RSL as inferred from the geological record at each study site, and this value represents the influence of vertical land motion (VLM) from all local processes. Some processes cannot be quantified (e.g. tidal range changes) and are assumed the same as modern; however, in order to compare against our ensemble of GIA and Antarctic melt scenarios, we subtract the influence of dynamic topography (VLM due to mantle convection), and in the case of offshore North Sea data points, subsidence due to sediment loading, from each record, assuming that active tectonics make a negligible contribution given the distance from active plate margins. By converting the magnitude of dynamic topography since 125 ka into a rate, we utilise the Austermann et al. [48] dataset to estimate the dynamic topography contribution to RSL for the WALIS data points, assuming the mean age for absolute ages and the mid-value for relative ages. Similarly, we consider the contribution of sediment loading in the southern North Sea where significant sediment has accumulated over the Quaternary [49, 50], using the rates fields provided by Cohen et al. [46]. Fig 4 shows the resulting time series of data-point values plotted for each sea-level region after correcting for the VLM factors, with the exception of GIA. In this form, the database of sea-level records and their corresponding values can be compared against our modelled RSL values through a model-data comparison process known as history matching.

Sea-level data-matching framework

History matching is a procedure used in model uncertainty quantification to rule out areas of the model parameter space (i.e. combinations of input parameter values) that are unable to match observational data within the bounds of model and data uncertainty [51–53]. To compare model output and observational data, we use an implausibility metric, as employed by Pollard et al. [33], which effectively calculates the minimum distance in space and time between the modelled RSL time-series and a sea-level data point, normalised by uncertainty. For each simulation we run, we calculate an implausibility value based on the normalised distance between the model and observations. Let y be the real-world value of some quantity and z be an observation of y that differs by an error e such that $z = y + e$. Our numerical model can make a prediction of y with some parameter combination $\hat{p}$, given by $f(\hat{p})$, but since our numerical model is not a perfect representation of the real world, all predictions $f(\hat{p})$ are separated from y by model structural discrepancy ϵ such that, for the hypothetical perfect parameter combination $\hat{p}^*$, $y = f(\hat{p}^*) + \epsilon$. Therefore, $E(\epsilon)$, the expectation of ϵ, represents the model bias and $E(\epsilon) \neq 0$ indicates that $f(\hat{p})$ contains a systematic bias from observation z. In the case that f is an emulated quantity from our original numerical model, we additionally define the emulator uncertainty $Var(f(\hat{p}))$. The implausibility $I(\hat{p})$ of a parameter combination $\hat{p}$ is therefore given by,

$$I(\hat{p}) = \sqrt{\frac{(E(f(\hat{p})) - z - E(\epsilon))^2}{Var(e) + Var(\epsilon) + Var(f(\hat{p}))}} \tag{2}$$

A RSL data point i consists of a location $\hat{x}_i$, RSL value z_i^{RSL}, an age z_i^t, and a data type. Implausibility calculations of RSL model outputs must, therefore, account for the RSL implausibility I_i^{RSL}, temporal implausibility I_i^t, and use a different form of this function to account for the specific interpretation of each RSL and age-data type. We assume that only model values at location x_i are relevant for calculating the implausibility of data point i, and therefore let $f_i(\hat{p}, t) \equiv f(\hat{p}, t, \hat{x} = x_i)$, where t is a modelled time from the discrete set of model times T. In addition, since we are only interested in LIG simulations, we only consider the subset of modelled RSL values that fall within T_{LIG}, where $T_{LIG} = \{t \in T | t \leq 129 \text{ ka and } t \geq 116 \text{ ka}\}$.

Beginning with the temporal implausibility, a sea-level data point can be associated with either an absolute age or a relative age. In the case of absolute ages, we assume that the age probability is normally distributed centred around the reported age z_i^t with standard deviation given by reported uncertainty $\sqrt{Var(e_i^t)}$. Using Equation 2 and assuming no temporal model bias or structural uncertainty, we define $I_i^t(t)$ for absolute ages to be,

$$I_i^t(t) = \sqrt{\frac{(t - z_i^t)^2}{Var(e_i^t)}} \tag{3}$$

In the case of relative ages, the temporal probability distribution is assumed as uniform between the lower bound t_{min} and the upper bound t_{max} of the reported age range, such that,

$$I_i^t(t) = \begin{cases} 0, \text{ if } z_i^{t_{min}} \leq t \leq z_i^{t_{max}} \\ \infty, \text{ else} \end{cases} \tag{4}$$

The RSL component of a data point can either be an index point, marine limiting, or terrestrial limiting. In the case of a sea level index point, RSL is assumed to be normally distributed and centred around the reported RSL value z_i^{RSL} with standard deviation given by reported uncertainty $\sqrt{Var(e_i^{RSL})}$. In this case, we can use Equation 2 to express I_i^{RSL} as,

$$I_i^{RSL}(\hat{p},t) = \sqrt{\frac{(E(f_i(\hat{p},t)) - z_i^{RSL} - E(\epsilon_i^{RSL}))^2}{Var(e_i^{RSL}) + Var(\epsilon_i^{RSL}) + Var(f_i(\hat{p},t))}}. \tag{5}$$

Limiting data points

In the case of a limiting data point, a RSL observation value z^{RSL} represents the boundary between possible and impossible RSL values and, by extension, $Var(z^{RSL})$ represents uncertainty in the position of this boundary. Consider a RSL value at some distance above an uncertain marine limiting RSL boundary: the probability of the RSL value represents the cumulative probability of all boundary values below it whereas a RSL value above this limit is only possible for boundary positions above it. By extension, we expect that a RSL value exactly on the mean of a normally distributed boundary position should have a probability of 0.5. Using this interpretation, the probability distribution of a modelled value f around this limit can be represented as the cumulative distribution function of a normal distribution. However, in order to include this alternative probability distribution within our history-matching framework we must first think of the standard implausibility of a model value f as, effectively, the distance, in terms of standard deviations, that this value lies away from the mean of a normal distribution given by,

$$N\left(\mu = z + E(\epsilon), \sigma = \sqrt{Var(e) + Var(\epsilon) + Var(f(\hat{p}))}\right). \tag{6}$$

With this interpretation, there exists a normalised probability P associated with each I, that can be calculated from the normalised probability density function associated with Equation 6 such that,

$$P = e^{-\frac{1}{2}I^2}. \tag{7}$$

By solving Equation 7 for I, we can express I in terms of P such that,

$$I = \sqrt{-2\log(P)}. \tag{8}$$

Let CDF be the cumulative distribution function associated with Equation 6 and, therefore, for limiting data points we can express the probability P_{lim} of a modelled RSL value $f(\hat{p})$ as,

$$P_{lim}(f(\hat{p})) = \begin{cases} CDF(f(\hat{p})), \text{ if marine limiting,} \\ 1 - CDF(f(\hat{p})), \text{ if terrestrial limiting.} \end{cases} \tag{9}$$

Combining Equation 8 and Equation 9 we can calculate the associated I as,

$$I(\hat{p}) = \sqrt{-2\log P_{lim}(f(\hat{p}))}. \tag{10}$$

Combined implausibility

The implausibility $I_i(\hat{p},t)$ of a model value $f_i(\hat{p},t)$, representing the normalised model-data distance in time and space, is given by,

$$I_i(\hat{p},t) = \sqrt{(I_i^{RSL}(\hat{p},t))^2 + (I_i^t(t))^2} \tag{11}$$

Since a sea-level model ensemble member at a location $\hat{x}$ consists of a time series of RSL values, we characterise the overall implausibility of $\hat{p}$ against i as,

$$I_i(\hat{p}) = \min\{I_i(\hat{p},t) : t \in T_{LIG}\} \tag{12}$$

Finally, we combine implausibility from all data points i into a single average implausibility for a given set of parameter values $\hat{p}$ by,

$$I(\hat{p}) = \text{mean}\{I_i(\hat{p}) : i \in N\} \tag{13}$$

Estimating model structural discrepancy

A misfit between modelled RSL and data that is common to all ensemble members may indicate the presence of a structural model bias, such that $E(\epsilon) \neq 0$. We account for this bias in our implausibility metric by defining the terms $E(\epsilon^{RSL})$ and $Var(\epsilon^{RSL})$ in Equation 2. We make the assumption that $E(\epsilon^{RSL})$ and $Var(\epsilon^{RSL})$, for the LIG, are time-invariant spatial fields which we can sample from at each data location to derive $E(\epsilon_i^{RSL})$ and $Var(\epsilon_i^{RSL})$. Intuitively, this means that we assume modelled RSL may be more incorrect in some locations than others but that there is no change in this error as the LIG progresses. In reality, this bias may be larger at some times than others due to, for example, the influence of missing ice-sheet contributions. However, spatial data sparsity, when grouped by model time step would limit the temporal resolution at which these fields could be estimated. In order to estimate $E(\epsilon^{RSL})$ and $Var(\epsilon^{RSL})$ we first calculate the RSL discrepancy $d_i(\hat{p})$ at z_i^t such that,

$$d_i(\hat{p}) = f(\hat{p}, t = z_i^t) - z_i^{rsl} \tag{14}$$

with $d_i(\hat{p}) = 0$ if i is a limiting data point and $f(\hat{p}, t = z_i^t)$ falls on the 'possible' side of the limit boundary. By calculating $d(\hat{p}) = \text{mean}\{|d_i(\hat{p})| : i \in N\}$ we can determine the best fitting 10% of ensemble members P_{best}. We then assume that this discrepancy is representative of ϵ_i^{RSL} at each data-point location i such that $E(\epsilon_i^{RSL})$ and $Var(\epsilon_i^{RSL})$ are the mean and variance of the set $\{d_i(\hat{p}) : \hat{p} \in P_{best}\}$. In this form $E(\epsilon_i^{RSL})$ and $Var(\epsilon_i^{RSL})$ are only defined at locations i and so, to aid the physical interpretation of the structural discrepancy, we spatially interpolate onto the northwest Eurasian region using a 2D Gaussian Process with a Matern-52 kernel, the results of which are shown in the Model bias subsection.

Results and analysis

Relative sea-level ensemble

Our ensemble of 532 RSL outputs shows a distinctive, Eurasian ice-sheet-driven pattern of higher LIG RSL under areas previously loaded by the Eurasian ice sheet, with values exceeding 100 ± 20 m in regions such as the White Sea, and lower RSL beyond the former ice-sheet margins (Fig 5). Our ensemble has a high rate of RSL change, averaged over the whole LIG, of up to 10 mm yr^{-1} in the Greenland-Iceland-Norwegian (GIN) Seas region, while the English Channel, North Atlantic, and southern North Sea regions show more moderate rates of change of 2 mm yr^{-1}. As the LIG progresses, areas underneath the former ice-sheet load experience RSL fall as a result of isostatic rebound, averaging -3 mm yr^{-1} in the central North Sea region, and with regions such as the Barents-Kara sea experiencing rates higher than -20 mm yr^{-1}. Uncertainty in the rate of RSL change is highest in regions dominated by isostatic rebound, reaching ± 12 mm yr^{-1} in the Baltic Sea compared to just ± 3 mm yr^{-1} in the GIN Seas.

The variance of our ensemble is estimating the range of possible RSL values given the specified uncertainty in viscoelastic Earth structure, Eurasian ice-sheet volume during the Penultimate Deglaciation, and the LIG evolution of AIS. In subsequent sections, we utilise this ensemble to quantify the sensitivity of each region to the evolution of AIS (sensitivity analysis), as well as to identify the region of our input parameter space most able to match observations of RSL (history matching). Sensitivity analysis requires RSL model output values at specific locations within the parameter space, while history matching is aided by far larger ensemble sizes than is feasible to directly compute with the sea-level model. Therefore, to aid both analyses, we train a Gaussian process emulator for each of the 141 unique data locations so that we are able to approximate RSL values at each location, including quantified prediction uncertainty, for arbitrary parameter input combinations.

Regional sensitivity analysis

The variance in our ensemble of Eurasian RSL results from the combined, propagated uncertainty in all of our model parameters and the magnitude of each model parameter's contribution to this variance is spatially variable. In Pollard et al. [33], we attributed individual model-parameter contributions to this spatial pattern of uncertainty and found that viscoelastic Earth model parameters are typically dominant across Eurasia, while regions directly underneath ice-sheet loads are sensitive to respective regional volumes of the Eurasian ice sheet. Here, we perform an expanded and targeted sensitivity analysis that includes AIS parameters by performing a Sobol Sensitivity analysis [54, 55]. To do this, we sample a 1024-member Sobol sequence [55] from our suite of Gaussian process emulators to calculate Sobol sensitivity indices at all site locations in the filtered RSL database. This computes the "first order" sensitivity of modelled RSL to each input parameter at every data location (i.e. the effect of a single parameter relative to the effect of all parameters), as well as the effects of interactions between parameters included in the "total-order" sensitivites [54]. To simplify the analysis and interpretation, we sum the individual parameter sensitivity indices into three parameter groups: Earth model, Eurasian ice volume, and Antarctic ice melt scenario. Finally, for each parameter group, we calculate a mean sensitivity value for each region that represents the average contribution of a given parameter group to uncertainty at data sites within a given region (as defined in Fig 4). Crucially, this analysis allows us to determine the sensitivity of each region's data to AIS ice-sheet melt.

Our results show that uncertainty in the Earth model parameters is the dominant contributor to RSL uncertainty in most regions, with an average contribution across all regions of 80%, compared with 12% from Eurasian ice-sheet volume and 3% from Antarctica (note that first-order contributions do not sum to 100% due to the influence of parameter interactions) as shown in Fig 6. The influence of GIA is particularly dominant in Greenland, likely due to lower influence from Eurasian ice-sheet changes, and in the North Sea, where it averages 91% across the Denmark, French North Sea, and Netherlands regions. The volume of the Eurasia ice sheet contributes little first-order sensitivity in these same North Sea regions, averaging 5%, but is far more dominant in the North Baltic Sea, South Baltic Sea, and White Sea regions, averaging 25%. By contrast, we find that the sensitivity to the Antarctic contribution is localised to the southwest subset of our sea-level regions where it contributes 6% to the English Channel, 4% to the English North Sea, 6% to the French Atlantic, and 16% to Wales.

Our sensitivity analysis results indicate that data points within the southwest subset of our Eurasian RSL data regions (Fig 4) are most sensitive to our parameterisation of AIS melt and, as such, are likely to be most informative about Antarctic melt scenarios. We now compare our ensemble with our refined database of RSL data points in order to: (i) identify regions of systematic misfit between model and data; (ii) filter out ensemble members that do not fit the sea-level data within uncertainty; (iii) identify AIS melt scenarios and Earth model configuration that best fit the data (in the Ensemble history matching subsection).

Model bias

The model bias term ϵ^{RSL}, as discussed in the Sea-level data-matching framework subsection, reflects the systematic misfit between modelled and observed values of RSL. In this work, we assume that ϵ^{RSL} is a spatially variable, temporally invariant field that we estimate by calculating the discrepancy between the mean modelled RSL value of the top 10% of ensemble members based on their fit against all data points following [32]. This field is used to correct our ensemble of RSL values in locations where the systematic misfit causes the RSL ensemble to be far from the data points, thus allowing all sea-level data to fairly inform our history-matching procedure. We find that our model exhibits spatially coherent patterns of ϵ^{RSL}, demonstrating both that the empirical RSL data is regionally consistent in its measurements of RSL and that our model contains biases, likely due to misrepresented ice-sheet volume and Earth model structure, on a regional scale.

We find that data points within the North Sea regions have a localised, negative mean model bias of $\mathcal{O}(50)$ m (of the order of 50 m), indicating that our ensemble of modelled RSL is higher than is suggested by the RSL data in these regions. However, this negative mean bias does not extend to the adjacent English Channel, Norwegian North Sea, or southern Baltic Sea region data points (Fig 7A). Within North Sea regions, the standard deviation (or uncertainty) of the model bias (or model structural error) is higher for data points in the Netherlands region, reaching $\mathcal{O}(10)$ m, whereas the English North Sea has an uncertainty of only $\mathcal{O}(2)$ m (Fig 7B). Both the mean and uncertainty in the model bias are negligible for data points in the English Channel, French Atlantic, and Wales regions, indicating that there is a reasonable intersection between our modelled range of RSL values and data points in these regions. Most data points in the eastern data regions of Svalbard, the Norwegian North Sea, southern Baltic Sea, northern Baltic Sea, White Sea, and the central Barents-Kara Sea also show negligible mean bias, although the higher proportion of limiting data points in this region may make these data points less able to constrain any bias. However, there is a large bias variance in the northern Baltic Sea of $\mathcal{O}(10)$ m, indicating that the best-fitting subset of our ensemble has high variability in this region. The North Barents-Kara Sea and Greenland regions have a strong positive bias of $\mathcal{O}(50)$ m with low accompanying uncertainty $\mathcal{O}(2)$ m, indicating that our modelled RSL values are systematically lower than expected in this region and that this correction is reasonably uniform across the best-fitting subset of ensemble members.

Ensemble history matching

Utilising our RSL ensemble, model-bias correction, and filtered subset of the WALIS sea-level database, we calculate the implausibility of a given sea-level model input parameter combination, with lower implausibility values corresponding to a closer model-data agreement. To perform this assessment, we utilise our suite of Gaussian process emulators to perform a 10^4-member LHS of our parameter space at each of the 141 unique data locations. The resulting 10^4 generated LIG RSL time series are compared against the 317 data points via the history matching methodology outlined in the Sea-level data-matching framework subsection to calculate the implausibility value $I_i(\hat{p})$ corresponding to each parameter sample $\hat{p}$ at each location i. In order to determine the resulting overall implausibility $I(\hat{p})$ associated with each $\hat{p}$ we then calculate the mean implausibility over all i for each $\hat{p}$. In addition, since our goal is to refine parameters describing scenarios of AIS melt, we utilise the information gained from our sensitivity analysis to perform a more selective history-matching procedure using only the subset of i that fall within regions most sensitive to AIS parameters: the English Channel, English North Sea, French Atlantic, and Wales. This reduced data subset contains 70 data points (43 more than those used by Barnett et al. [27]) consisting of 52 sea-level index points, 6 marine limiting, and 12 terrestrial limiting points, of which 37 and 33 are associated with absolute and relative ages, respectively.

The average implausibility of all parameter combinations against all data is 1.4, and the average implausibility against the AIS sensitive regional subset 1.2, while the maximum implausibility in our ensemble is 2.9. This means that all parameter combinations tested have an average implausibility within the 3-sigma uncertainty threshold Pukelsheim et al. [56] typically used in history matching [57, 58] and, as a result, all parameter combinations are deemed NROY when compared against all RSL data. However, despite the classification as NROY, differences in implausibility values between sample members can still be used to extract useful information about preferred parameter distributions. We therefore use the 10% subset of our parameter sample with the lowest implausibility values as representative of the best-fitting subset of parameters and refer to this subset as the refined subset.

Our refined parameter space, history matched against all data regions (blue distributions in Fig 8), shows a clear preference for lower ν_{UM} values than our original range, with a mean value of 2.2×10^{20} Pa s and an upper value of 4.1×10^{20} Pa s (99th percentile), falling well below the original uniform upper bound of 10×10^{20} Pa s. We find that the higher ν_{LM} values of our original uniform range are preferred, with the lower 1st percentile falling at 1×10^{22} Pa s compared with the original 0.1×10^{22} Pa s lower bound, with the mean value shifting to 3×10^{22} Pa s. Lower values of L are preferred, but the 95th percentile still lies at 94×10^3 km and, therefore, remains close to the original upper bound of 100×10^3 km, while the mean has shifted to 84×10^3 km. The regional subset shows similar overall preferences for Earth model parameters but has a stronger preference for lower ν_{UM} with a mean and 99th percentile of 1.7×10^{20} Pa s and 2.9×10^{20} Pa s, respectively. We also find values close to the upper bound of ν_{LM} are less preferred and the L refined distribution is more similar to that of the original uniform sample.

Our full-data history matching prefers larger Barents-Kara Sea ice-sheet volume, with the V_{BKS} distribution shifting from an original 28 ± 4 m SLE (mean $\pm$ standard deviation as a normal distribution) to 30 ± 3 m SLE. By contrast, there is no change within uncertainty in the preferred V_{BI} distribution, while the V_F shows a preference for a small regional ice-sheet load, reducing from 24 ± 3 m SLE to 22 ± 3 m SLE. The regional subset shows no change in the refined normal distributions for regional Barents-Kara Sea, British-Irish, or Fennoscandian Eurasian ice-sheet volume, within uncertainty. Our history-matching procedure reveals no significant preference for parameters controlling the timing or duration of WAIS or EAIS LIG evolution, with T^{EA}_{change}, d^{EA}_{change}, T^{WA}_{melt}, T^{WA}_{melt}, and d^{WA}_{stable} following similar distributions as the original sample. However, refined distributions from both all data regions and the subset of regions sensitivity to AIS changes reveal preferences for higher ice-sheet melt contributions for both V^{WA}_{melt} and V^{EA}_{change}. Our sensitive subset suggests a contribution of 0.5 - 4.9 m from WAIS (*very likely*, 90th percentile) and -0.4 - 4 m from EAIS (*very likely*) but prefers higher volume contributions of 2.1 - 4.9 m from WAIS (*likely*, 66th percentile) and 1.1 - 4.4 m from EAIS (*likely*), and thus a total AIS melt contribution of 3.2 - 9.3 m (*likely*). These results show that high ice-sheet melt from EAIS and/or WAIS produce lower values of model implausibility. However, we find that our results cannot distinguish between an East and West source of melt and this is investigated in the Discussion.

Our resulting posterior parameter distributions for AIS scenarios, history matched against regionally sensitive data, can be inverted to produce a refined ensemble of AIS melt scenarios (Fig 9), demonstrating the range of tested AIS scenarios best able to match the AIS sensitive subset of northwest Eurasian RSL data.

Discussion

Antarctic melt-scenario methodology

We have simulated Eurasian RSL during the LIG using a range of possible scenarios for LIG AIS evolution via our new parameterisation of AIS melt scenarios. This parameterisation has allowed us to systematically test the timing, duration, and magnitude of LIG WAIS and EAIS volume changes based on ice-sheet thickness configurations from the Deconto et al. [30] model. Our simple approach made use of dynamic ice-sheet model outputs in an experimental design that differs in several ways from traditional dynamic ice-sheet modelling studies. Firstly, by utilising a pre-existing set of ice-sheet configurations, each ice-sheet input to our sea-level model is computationally inexpensive to assemble, allowing for the execution of our large-ensemble experimental design that would otherwise be computationally challenging with a coupled climate-ice model without the use of coarse model grids [59], simplified climate inputs [14], or model emulation [29]. Secondly, we are able to test a greater range of possible ice-sheet melt scenarios than may be possible with the use of dynamic ice-sheet models since the range of ice-sheet evolutions produced by such models is constrained by the choice of implemented model physics [2]. While in-built model physics provides useful constraints on possible ice-sheet configurations, this range is dependent on the particular model's choice of included ice-sheet physical processes, the specific numerical implementation of these processes, and the range of model boundary conditions tested [60–62]. In the context of the LIG, a lack of observations of the AIS physical response to changes in the ocean and climate system, and the resulting large uncertainties on dynamic model boundary conditions and parameterisation of physical processes, can cast doubt on the reliability of dynamic model-based constraints from a single model on ice-sheet behaviour [63–65].

While our approach allows for flexibility in the range of scenarios tested it also requires prior assumptions to be made about suitable distributions of the timing, duration, and volume of LIG AIS changes, based upon previous work and understanding of WAIS and EAIS dynamics. Our range of d^{WA}_{melt} values allows for rapid WAIS retreat of up to 0.5 ka and reflects the view of previous work that the WAIS has the potential for rapid ice-sheet loss [66]. The Antarctic BUttressing model Intercomparison Project (ABUMIP) of Sun et al. [67] investigated possible rates of AIS mass loss from grounding line retreat, including marine ice sheet instability (MISI) and MICI effects, and found multi-meter retreats over $\mathcal{O}(0.5)$ ka in all sensitivity experiments. While basins within the EAIS may also be subject to rapid responses to ocean and climate forcing they make up a smaller portion of the ice-sheet mass and, as such, we prescribe a more moderate minimum bound for d^{EA}_{change} of 1 ka since the rate of EAIS overall mass loss is therefore likely to be lower. There is little agreement as to the timing of initial LIG WAIS and EAIS melt, as well as the duration and timing of ice-sheet growth, and so we allow a 5 ka window for the initiation of LIG retreat, beginning at 129 ka, for both ice sheets, while also allowing a wide time window for the duration of ice growth. After running the sea-level model ensemble, our original sample of SLE contribution parameters, ranging from 0 - 5.5 m for V^{WA}_{melt} and -5 to 5 m for V^{EA}_{change}, were corrected to account for LIG topography changes, shifting their ranges to -0.25 - 5m for V^{WA}_{melt} and -1.2 - 4.5 m for V^{EA}_{change} (in the Relative sea-level ensemble subsection). After this correction, our volume ranges encompass the majority of projected ranges of mass loss from dynamic ice-sheet modelling studies of 1 - 5 m for WAIS [11, 17–19] and -1 to 5 m for EAIS [23, 44], providing a independent constraint on these likely ice-sheet contribution during the LIG. Uplift from GIA-driven Antarctic topography deformation during the

LIG may act to reduce the volume of the surrounding ocean basin thus driving additional GMSL rise, a process known as water expulsion, which may represent an underestimation of up to 30% from our sea-level contribution values for a given AIS scenario [20].

Regional sensitivity

We have quantified the relative sensitivity of RSL within different regions of Eurasia to changes in the LIG AIS, uncertainty in the viscoelastic Earth model and uncertainties in the Penultimate Deglaciation of the Eurasian ice sheet. We found that, in most regions, AIS uncertainty was dwarfed by the considerable contribution of regional GIA uncertainty and that AIS influence was only pronounced in the regions in our study area far from local ice-sheet changes. Among these regions, Wales had the largest sensitivity to AIS changes, likely due to the relatively small load from the British-Irish ice sheet reducing both the direct influence of ice-sheet volume uncertainty as well as consequential influences of viscoelastic deformation. The French Atlantic, English Channel, and English North Sea regions also exhibit proportionally high influence from AIS and, as they are less proximal to centres of large Eurasian ice-sheet load, thus lowering sensitivity to Eurasian ice-sheet volume. Our conclusions suggest that the southwest subset of our Eurasian data regions (Fig 4) has the potential to be more informative about AIS than other Eurasian regions when utilised in model-data comparison studies since the greatest proportion of the observed RSL values and regional model uncertainty can be explained by AIS melt.

History matching

In order to quantify the fit of our RSL ensemble against the northwest Eurasian subset of the WALIS sea-level database, we calculated the implausibility of our parameter space using a bespoke Bayesian history-matching framework that accounts for uncertainty in observed and modelled RSL values, limiting data points, and model structural error and bias. Our results show that no areas of our explored parameter space are deemed as implausible within 3-sigma uncertainty. As such, we concluded that current uncertainties in temporal and RSL data values, combined with the magnitude of modelled RSL uncertainty, cannot decisively identify implausible modelled RSL scenarios and, by extension, AIS melt scenarios. Despite this, we have been able to deduce information within the subset of our parameter space with the lowest 10% implausibility and, within this subset, we observed a clear preference for the choice of viscoelastic Earth model, Eurasian ice-sheet volume, and the magnitude of AIS melt. In particular, low ν_{UM} values in the best-fitting subset, contain virtually no model runs with ν_{UM} greater than 5×10^{20} Pa s, suggesting a lower viscosity Earth structure and, as a result, more pronounced (and more rapid) deformation is better able to match observational data. Our results also indicate that a thinner Eurasian lithosphere is more likely, preferring lower values of L (70×10^3 - 85×10^3 km, 66th percentile) in our full-regional history matching, combined with low ν_{UM}, although these preferences are not expressed by our southwest regional subset. The post-Last Glacial Maximum (LGM) and Holocene British-Irish ice sheet focused GIA study of Bradley et al. [38] also showed a slight preference for higher ν_{LM} values of between 3×10^{22} Pa s and 5×10^{22} Pa s but, in contrast to our results, found a slightly better model-data fit for runs with higher ν_{UM} values of 5×10^{20} Pa s as opposed to 3×10^{20} Pa s. However, some of this difference in viscosity preference could be explained by the differences in British-Irish ice-sheet volumes between our PGM simulations and the Bradley LGM model. Our full-regional history matching also showed a pronounced preference for higher volumes of the V_{BKS}, suggesting that RSL data in the Barents-Kara Sea region have undergone high levels of subsidence. In contrast, a preference for lower V_F suggests that our mean ice-sheet load in Fennoscandia may be driving subsidence rates larger than indicated by observational constraints and, thus, our ice-sheet model may be too thick in this region.

We did not find significant preferences for parameters controlling the timing or duration of AIS mass changes and this is likely a result of the large temporal uncertainties present in the RSL data points. However, we found a clear preference for high values of melt from both V^{WA}_{melt} and V^{EA}_{change}, especially from the subset of data regions sensitive to AIS melt. However, it is not clear from this analysis whether Eurasian sea-level data is sensitive to EAIS and WAIS sea-level contributions seperately, or simply the total AIS contribution. In order to determine whether distinct preferences for EAIS and WAIS contributions can be disentangled, we perform a pairwise implausibility calculation to identify any differences in implausibility values for equal total AIS melt contributions composed of different EAIS and WAIS contributions (Fig 10). Each pixel within Fig 10 represents the average implausibility for fixed values of both WAIS and EAIS sea-level contribution, indicated by cell position, over a 1000-member random sample of all other parameters. We used a 30-part, linear discretisation of EAIS and WAIS value ranges, resulting in a 30 by 30 pixel matrix, totalling 900 pixels and representing the evaluation of 9×10^9 parameter combinations with each of our Gaussian process emulators. Our results do not show a major distinction in preference between equal total AIS contributions with differing EAIS and WAIS contributions, and thus we conclude that it is currently not possible to distinguish the AIS source of ice-sheet melt with our current model framework and available data.

Model bias

In history matching our ensemble, we accounted for the spatial pattern of the model structural error and bias, allowing the extraction of useful information from RSL records even in regions where there exists a consistent model-data mismatch. Our methodology allows us to transparently present the regional shortcomings of our model for interpretation and targeted future improvement. Prior to correcting for this systematic model bias, we found that the current range of ice-sheet and viscoelastic Earth model parameters were unable to match RSL values inferred by some rate-corrected observational records in the WALIS database. We estimated the model bias at each location by calculating the average discrepancy between the overall best-fitting 10% of ensemble members (against all records) and each sea-level record. In addition, we performed a 2D interpolation procedure in order to estimate the spatial structure of the model bias and aid interpretation, thus revealing a strong spatial structure to the model-data discrepancy. In particular, we found that modelled RSL in the southern North Sea region is over-estimated; RSL at sites beneath the former Eurasian ice sheet tended to be under-estimated; and records in the North Atlantic, English Channel and Wales regions showed good fit against our model. We found that the mean shift in parameter ranges controlling the Earth's viscoelastic structure was strongly controlled by the region against which they were compared, revealing that no one Earth model parameter combination can best match all Eurasian LIG RSL data. Instead, our work shows the importance of a spatially varying Earth structure and, in future work, we suggest that studies may need to incorporate 3D Earth models into their analysis.

The discrepancy between data and our modelled North Sea RSL may reflect an overestimation of ice-sheet thickness in this region as generated by our ensemble of Eurasian Penultimate Deglaciation geometries calculated using a simple ice-sheet model [32, 68]. This portion of the Eurasian ice sheet is known to be difficult to simulate during the Last Deglaciation, even when applying more complex ice-sheet models and available greater data constraints, due to the strong influence of dynamic ice-sheet processes that control the separation of the British-Irish and Fennoscandian ice sheet sectors and the influence of the deep Norwegian channel [69–72]. In addition to being influenced by variation in Earth's viscosity structure, model-data discrepancy may also be influenced by the assumption of a single Eurasian PGM ice-sheet margin for all ensemble members. Pollard et al. [33] found some regional sensitivity to parameters controlling the asynchrony of ice-sheet margin retreat but, since this sensitivity was relatively localised to some areas of the Barents-Kara Sea, we removed parameters controlling this influence to reduce the size of our parameter space. As a result, reintroducing this parameterisation and expanding the assessment of margin extent and timing uncertainty to other areas of the ice-sheet margin may help to improve model-data fit in locations proximal to the ice-sheet margin.

Alternative sources of Last Interglacial sea-level rise

LIG GrIS mass-loss estimates generally are thought to be lower than those of the AIS with most studies estimating a contribution of between 0.6 and 3.5 m SLE [5, 14, 73, 74] but higher contributions from GrIS of +5 m have also been suggested [15, 16]. In this work, we assume that Greenland ice-sheet melt during the LIG had a relatively small impact on Northwest European RSL values when compared against AIS [27, 75]. In order to validate this assumption we performed an additional simulation that focused on LIG Greenland ice-sheet melt. As input, we used the Greenland LIG deglaciation model of Sommers et al. [74], which runs from 127 ka to 119 ka, as the Greenland component in our global ice-sheet model. We followed the same procedure as used for simulating AIS melt, whereby all other ice-sheets (including AIS) were kept in their pre-industrial configurations throughout the LIG, but we allowed the ice-sheet model to follow it's original temporal evolution. We used our interpolation methodology to smoothly join the final Sommers et al. [74] Greenland ice-sheet configuration at 119 ka with the pre-industrial configuration at 116 ka. Since we simulated a single evolution of the Greenland ice-sheet, we selected single Earth model and Eurasian ice-sheet model ensemble members that lay closest to the ensemble mean. Our results showed that Greenland contributed up to 1 m of RSL change in the southern North Sea and Baltic Sea, reducing to up to 0.5 m in the northern North Sea and across the northern Fenoscandian coastline, in keeping with the results of Hay et al. [25]. While our work does not encompass a full probabilistic estimation of the Greenland contribution, these results demonstrate the limited value that the inclusion of a parameterised Greenland would make to our final results.

In order to simplify the identification of Antarctic influence, our work also assumes that all other terrestrial ice-sheet deglaciation (e.g. Laurentide) are complete prior to the LIG and thus do not directly contribute to ocean water volume changes. However, Zhou et al. [76] have suggested that the Laurentide ice sheet may have persisted into the LIG, indicated by a Laurentide outburst flood event at 125 ka. Based on this work and the pattern of LIG RSL in some far-field records Creel et al. [13, 77] have proposed that the Laurentide may have contributed to ongoing LIG melt. Furthermore, if the thermal expansion contribution estimate of 0.4 ± 0.3 m from Mckay et al. [10] and mountain glacial melt contribution estimate of 0.32 ± 0.08 m SLE from Marzeion et al. [12] are considered they may, combined, lower our AIS LIG contribution estimate by 0.7 ± 0.4 m, but this correction value is small compared against RSL data uncertainty. It is therefore plausible that a small proportion of our attributed AIS contribution may, in fact, be due to the combined influence of GrIS and Laurentide melt, alongside thermal expansion, and a more comprehensive assessment of these contributions should be explored in future work.

Conclusions

Significant uncertainties in both observational constraints and modelled simulations make model-data comparison studies of LIG RSL a significant challenge, particularly when focused on identifying AIS ice-sheet melt. To address this problem, we developed a simple parameterisation of AIS LIG evolution that specifies the timing, duration, and magnitude of WAIS and EAIS ice-sheet changes and used this to produce a 532-member ensemble of Eurasian LIG RSL simulations that vary in viscoelastic Earth structure, the Penultimate Deglaciation of the Eurasian ice sheet, and AIS evolution. We utilise sensitivity analysis to quantify the contribution of AIS uncertainty to the variance in 15 regions of northwest Eurasian and found that AIS sensitivity was concentrated in the southwestern sector of these study areas, particularly in the English Channel, English North Sea, French Atlantic, and Wales. We compared our ensemble of RSL against data contained within the state-of-the-art WALIS RSL database [31] by using a comprehensive history-matching framework that accounts for structural errors in our numerical model, parameter space uncertainty, and both age and RSL uncertainty in observational constraints. In addition, we expanded this framework to incorporate information from limiting RSL data points as well as those associated with relative age constraints. Our history-matching procedure allowed us to determine the implausibility of our parameter space and, after correcting for regional model bias, we found that all of our model outputs were able to fit sea-level data within 3-sigma uncertainty.

Despite not being able to explicitly rule out portions of our parameter space, individual parameter combinations could still be compared by their relative implausibility values. When compared against RSL data within regions sensitive to AIS melt, the best-fitting 10% subset of our parameter space shows a distinct preference for high values of AIS melt, but cannot distinguish between East and West Antarctic contributions. In addition, our refined viscoelastic earth model parameter distributions showed a strong preference for low upper mantle viscosity values as well as moderate preferences for thin lithospheric thickness values and higher values of lower mantle viscosity. However, we find evidence for differences in regional viscoelastic parameter preferences, indicating a need to account for a spatially varying Earth structure across the Eurasian region. To conclude, our work suggests that, of all northwest Eurasian regions that we have considered, RSL data within the English Channel, Wales, and French Atlantic regions are most sensitive to AIS melt and that a high total AIS melt contribution of 3.2 - 9.3 m (*likely*, 66th percentile) is best able to explain this RSL data. However, a greater quantity of high-quality, low-uncertainty RSL data points in regions sensitive to the AIS sea-level fingerprint, combined with more detailed assessments of temporal constraints, are needed to be able to rule out models of RSL and make decisive conclusions about the most likely patterns of LIG AIS evolution.

References

1. IPCC. The Ocean and Cryosphere in a Changing Climate: Special Report of the Intergovernmental Panel on Climate Change. Cambridge: Cambridge University Press; 2022. doi:10.1017/9781009157964.
2. Pattyn F, Morlighem M. The Uncertain Future of the Antarctic Ice Sheet. Science. 2020 Mar;367(6484):1331-5. doi:10.1126/science.aaz5487.
3. Robel AA, Seroussi H, Roe GH. Marine Ice Sheet Instability Amplifies and Skews Uncertainty in Projections of Future Sea-Level Rise. Proceedings of the National Academy of Sciences. 2019 Jul;116(30):14887-92. doi:10.1073/pnas.1904822116.
4. Capron E, Govin A, Stone EJ, Masson-Delmotte V, Mulitza S, Otto-Bliesner B, et al. Temporal and Spatial Structure of Multi-Millennial Temperature Changes at High Latitudes during the Last Interglacial. Quaternary Science Reviews. 2014 Nov;103:116-33. doi:10.1016/j.quascirev.2014.08.018.
5. Otto-Bliesner BL, Marshall SJ, Overpeck JT, Miller GH, Hu A, CAPE Last Interglacial Project members. Simulating Arctic Climate Warmth and Icefield Retreat in the Last Interglaciation. Science. 2006 Mar;311(5768):1751-3. doi:10.1126/science.1120808.
6. Kopp RE, Simons FJ, Mitrovica JX, Maloof AC, Oppenheimer M. Probabilistic Assessment of Sea Level during the Last Interglacial Stage. Nature. 2009 Dec;462(7275):863-7. doi:10.1038/nature08686.
7. Dutton A, Carlson AE, Long AJ, Milne GA, Clark PU, DeConto R, et al. Sea-Level Rise Due to Polar Ice-Sheet Mass Loss during Past Warm Periods. Science. 2015 Jul;349(6244):aaa4019. doi:10.1126/science.aaa4019.
8. Dyer B, Austermann J, D'Andrea WJ, Creel RC, Sandstrom MR, Cashman M, et al. Sea-Level Trends across The Bahamas Constrain Peak Last Interglacial Ice Melt. Proceedings of the National Academy of Sciences. 2021 Aug;118(33):e2026839118. doi:10.1073/pnas.2026839118.
9. Fox-Kemper B, Hewitt HT, Xiao C, Aealgeirsdóttir G, Drijfhout SS, Edwards TL, et al. Ocean, Cryosphere and Sea Level Change. In: Masson-Delmotte V, Zhai P, Pirani A, Connors SL, Péan C, Berger S, et al., editors. Climate Change 2021: The Physical Science Basis. Contribution of Working Group I to the Sixth Assessment Report of the Intergovernmental Panel on Climate Change. Cambridge, United Kingdom and New York, NY, USA,: Cambridge University Press; 2021. p. 1211-362. doi:10.1017/9781009157896.011.
10. McKay NP, Overpeck JT, Otto-Bliesner BL. The Role of Ocean Thermal Expansion in Last Interglacial Sea Level Rise: THERMAL EXPANSION IN LIG SEA LEVEL RISE. Geophysical Research Letters. 2011 Jul;38(14):n/a-n/a. doi:10.1029/2011GL048280.
11. Turney CSM, Fogwill CJ, Golledge NR, McKay NP, van Sebille E, Jones RT, et al. Early Last Interglacial Ocean Warming Drove Substantial Ice Mass Loss from Antarctica. Proceedings of the National Academy of Sciences. 2020 Feb;117(8):3996-4006. doi:10.1073/pnas.1902469117.
12. Marzeion B, Hock R, Anderson B, Bliss A, Champollion N, Fujita K, et al. Partitioning the Uncertainty of Ensemble Projections of Global Glacier Mass Change. Earth's Future. 2020;8(7):e2019EF001470. doi:10.1029/2019EF001470.

13. Creel RC, Austermann J. Glacial Isostatic Adjustment Driven by Asymmetric Ice Sheet Melt during the Last Interglacial Causes Multiple Local Sea-Level Peaks. Geology. 2024 Dec. doi:10.1130/G52483.1.

14. Stone EJ, Lunt DJ, Annan JD, Hargreaves JC. Quantification of the Greenland Ice Sheet Contribution to Last Interglacial Sea Level Rise. Climate of the Past. 2013 Mar;9(2):621-39. doi:10.5194/cp-9-621-2013.

15. Yau AM, Bender ML, Robinson A, Brook EJ. Reconstructing the Last Interglacial at Summit, Greenland: Insights from GISP2. Proceedings of the National Academy of Sciences. 2016 Aug;113(35):9710-5. doi:10.1073/pnas.1524766113.

16. Cuffey KM, Marshall SJ. Substantial Contribution to Sea-Level Rise during the Last Interglacial from the Greenland Ice Sheet. Nature. 2000 Apr;404(6778):591-4. doi:10.1038/35007053.

17. DeConto RM, Pollard D. Contribution of Antarctica to Past and Future Sea-Level Rise. Nature. 2016 Mar;531(7596):591-7. doi:10.1038/nature17145.

18. Clark PU, He F, Golledge NR, Mitrovica JX, Dutton A, Hoffman JS, et al. Oceanic Forcing of Penultimate Deglacial and Last Interglacial Sea-Level Rise. Nature. 2020 Jan;577(7792):660-4. doi:10.1038/s41586-020-1931-7.

19. Golledge NR, Clark PU, He F, Dutton A, Turney CSM, Fogwill CJ, et al. Retreat of the Antarctic Ice Sheet During the Last Interglaciation and Implications for Future Change. Geophysical Research Letters. 2021;48(17):e2021GL094513. doi:10.1029/2021GL094513.

20. Pan L, Powell EM, Latychev K, Mitrovica JX, Creveling JR, Gomez N, et al. Rapid Postglacial Rebound Amplifies Global Sea Level Rise Following West Antarctic Ice Sheet Collapse. Science Advances. 2021 Apr;7(18):eabf7787. doi:10.1126/sciadv.abf7787.

21. Huybrechts P. Glaciological Modelling of the Late Cenozoic East Antarctic Ice Sheet: Stability or Dynamism? Geografiska Annaler: Series A, Physical Geography. 1993 Dec;75(4):221-38. doi:10.1080/04353676.1993.11880395.

22. Stokes CR, Abram NJ, Bentley MJ, Edwards TL, England MH, Foppert A, et al. Response of the East Antarctic Ice Sheet to Past and Future Climate Change. Nature. 2022 Aug;608(7922):275-86. doi:10.1038/s41586-022-04946-0.

23. Fogwill CJ, Turney CSM, Meissner KJ, Golledge NR, Spence P, Roberts JL, et al. Testing the Sensitivity of the East Antarctic Ice Sheet to Southern Ocean Dynamics: Past Changes and Future Implications: SENSITIVITY OF THE EAST ANTARCTIC ICE SHEET TO SOUTHERN OCEAN DYNAMICS. Journal of Quaternary Science. 2014 Jan;29(1):91-8. doi:10.1002/jqs.2683.

24. Bradley SL, Siddall M, Milne GA, Masson-Delmotte V, Wolff E. Combining Ice Core Records and Ice Sheet Models to Explore the Evolution of the East Antarctic Ice Sheet during the Last Interglacial Period. Global and Planetary Change. 2013 Jan;100:278-90. doi:10.1016/j.gloplacha.2012.11.002.

25. Hay C, Mitrovica JX, Gomez N, Creveling JR, Austermann J, E Kopp R. The Sea-Level Fingerprints of Ice-Sheet Collapse during Interglacial Periods. Quaternary Science Reviews. 2014 Mar;87:60-9. doi:10.1016/j.quascirev.2013.12.022.

26. Mitrovica JX, Gomez N, Clark PU. The Sea-Level Fingerprint of West Antarctic Collapse. Science. 2009 Feb;323(5915):753-3. doi:10.1126/science.1166510.

27. Barnett RL, Austermann J, Dyer B, Telfer MW, Barlow NLM, Boulton SJ, et al. Constraining the Contribution of the Antarctic Ice Sheet to Last Interglacial Sea Level. Science Advances. 2023 Jul;9(27):eadf0198. doi:10.1126/sciadv.adf0198.

28. Rohling EJ, Hibbert FD, Grant KM, Galaasen EV, Irvalı N, Kleiven HF, et al. Asynchronous Antarctic and Greenland Ice-Volume Contributions to the Last Interglacial Sea-Level Highstand. Nature Communications. 2019 Dec;10(1):5040. doi:10.1038/s41467-019-12874-3.

29. Gilford DM, Ashe EL, DeConto RM, Kopp RE, Pollard D, Rovere A. Could the Last Interglacial Constrain Projections of Future Antarctic Ice Mass Loss and Sea-Level Rise? Journal of Geophysical Research: Earth Surface. 2020 Oct;125(10). doi:10.1029/2019JF005418.

30. DeConto RM, Pollard D, Alley RB, Velicogna I, Gasson E, Gomez N, et al. The Paris Climate Agreement and Future Sea-Level Rise from Antarctica. Nature. 2021 May;593(7857):83-9. doi:10.1038/s41586-021-03427-0.

31. Rovere A, Ryan DD, Vacchi M, Dutton A, Simms AR, Murray-Wallace CV. The World Atlas of Last Interglacial Shorelines (Version 1.0). Earth System Science Data. 2023 Jan;15(1):1-23. doi:10.5194/essd-15-1-2023.

32. Pollard OG, Barlow NLM, Gregoire LJ, Gomez N, Cartelle V, Ely JC, et al. Quantifying the Uncertainty in the Eurasian Ice-Sheet Geometry at the Penultimate Glacial Maximum (Marine Isotope Stage 6). The Cryosphere. 2023 Nov;17(11):4751-77. doi:10.5194/tc-17-4751-2023.

33. Pollard OG, Barlow NLM, Gregoire LJ, Gomez N. Relative sea-level sensitivity in the Eurasian region to Earth and ice-sheet model uncertainty during the Last Interglacial. Quaternary Science Reviews. 2024;343:108908. Available from: `https://www.sciencedirect.com/science/article/pii/S0277379124004098`. doi:https://doi.org/10.1016/j.quascirev.2024.108908.

34. Han HK, Gomez N, Wan JXW. Capturing the interactions between ice sheets, sea level and the solid Earth on a range of timescales: a new "time window" algorithm. Geoscientific Model Development. 2022;15(3):1355-73.

35. Kendall RA, Mitrovica JX, Milne GA. On Post-Glacial Sea Level - II. Numerical Formulation and Comparative Results on Spherically Symmetric Models. Geophysical Journal International. 2005 Jun;161(3):679-706. doi:10.1111/j.1365-246X.2005.02553.x.

36. Milne GA, Mitrovica JX. Postglacial Sea-Level Change on a Rotating Earth: First Results from a Gravitationally Self-Consistent Sea-Level Equation. Geophysical Journal International. 1996 Sep;126(3):F13-20. doi:10.1111/j.1365-246X.1996.tb04691.x.

37. Mitrovica JX, Milne GA. On Post-Glacial Sea Level: I. General Theory. Geophysical Journal International. 2003 Aug;154(2):253-67. doi:10.1046/j.1365-246X.2003.01942.x.

38. Bradley SL, Ely JC, Clark CD, Edwards RJ, Shennan I. Reconstruction of the Palaeo-sea Level of Britain and Ireland Arising from Empirical Constraints of Ice Extent: Implications for Regional Sea Level Forecasts and North American Ice Sheet Volume. Journal of Quaternary Science. 2023 Apr:jqs.3523. doi:10.1002/jqs.3523.

39. Dendy S, Austermann J, Creveling JR, Mitrovica JX. Sensitivity of Last Interglacial Sea-Level High Stands to Ice Sheet Configuration during Marine Isotope Stage 6. Quaternary Science Reviews. 2017 Sep;171:234-44. doi:10.1016/j.quascirev.2017.06.013.

40. Milne Ga, Shennan I, Youngs Bar, Waugh Ai, Teferle Fn, Bingley Rm, et al. Modelling the Glacial Isostatic Adjustment of the UK Region. Philosophical Transactions of the Royal Society A: Mathematical, Physical and Engineering Sciences. 2006 Feb;364(1841):931-48. doi:10.1098/rsta.2006.1747.

41. Peltier WR, Argus DF, Drummond R. Space Geodesy Constrains Ice Age Terminal Deglaciation: The Global ICE-6G_C (VM5a) Model: Global Glacial Isostatic Adjustment. Journal of Geophysical Research: Solid Earth. 2015 Jan;120(1):450-87. doi:10.1002/2014JB011176.

42. Waelbroeck C, Labeyrie L, Michel E, Duplessy JC, McManus JF, Lambeck K, et al. Sea-Level and Deep Water Temperature Changes Derived from Benthic Foraminifera Isotopic Records. Quaternary Science Reviews. 2002 Jan;21(1-3):295-305. doi:10.1016/S0277-3791(01)00101-9.

43. Rignot E, Jacobs S, Mouginot J, Scheuchl B. Ice-Shelf Melting Around Antarctica. Science. 2013 Jul;341(6143):266-70. doi:10.1126/science.1235798.

44. Harig C, Simons FJ. Accelerated West Antarctic Ice Mass Loss Continues to Outpace East Antarctic Gains. Earth and Planetary Science Letters. 2015 Apr;415:134-41. doi:10.1016/j.epsl.2015.01.029.

45. Rovere A, Raymo ME, Vacchi M, Lorscheid T, Stocchi P, Gómez-Pujol L, et al. The Analysis of Last Interglacial (MIS 5e) Relative Sea-Level Indicators: Reconstructing Sea-Level in a Warmer World. Earth-Science Reviews. 2016 Aug;159:404-27. doi:10.1016/j.earscirev.2016.06.006.

46. Cohen KM, Cartelle V, Barnett R, Busschers FS, Barlow NLM. Last Interglacial Sea-Level Data Points from Northwest Europe. Earth System Science Data. 2022 Jun;14(6):2895-937. doi:10.5194/essd-14-2895-2022.

47. Dalton AS, Gowan EJ, Mangerud J, Möller P, Lunkka JP, Astakhov V. Last Interglacial Sea-Level Proxies in the Glaciated Northern Hemisphere. Earth System Science Data. 2022 Apr;14(4):1447-92. doi:10.5194/essd-14-1447-2022.

48. Austermann J, Mitrovica JX, Huybers P, Rovere A. Detection of a Dynamic Topography Signal in Last Interglacial Sea-Level Records. Science Advances. 2017 Jul;3(7):e1700457. doi:10.1126/sciadv.1700457.

49. Hijma MP, Cohen KM, Roebroeks W, Westerhoff WE, Busschers FS. Pleistocene Rhine–Thames Landscapes: Geological Background for Hominin Occupation of the Southern North Sea Region. Journal of Quaternary Science. 2012;27(1):17-39. doi:10.1002/jqs.1549.

50. Lamb RM, Harding R, Huuse M, Stewart M, Brocklehurst SH. The Early Quaternary North Sea Basin. Journal of the Geological Society. 2018 Mar;175(2):275-90. doi:10.1144/jgs2017-057.

51. Vernon I, Owen J, Aylett-Bullock J, Cuesta-Lazaro C, Frawley J, Quera-Bofarull A, et al. Bayesian Emulation and History Matching of JUNE. Philosophical Transactions of the Royal Society A: Mathematical, Physical and Engineering Sciences. 2022 Aug;380(2233):20220039. doi:10.1098/rsta.2022.0039.

52. Williamson D, Goldstein M, Allison L, Blaker A, Challenor P, Jackson L, et al. History Matching for Exploring and Reducing Climate Model Parameter Space Using Observations and a Large Perturbed Physics Ensemble. Climate Dynamics. 2013 Oct;41(7-8):1703-29. doi:10.1007/s00382-013-1896-4.

53. Bower RG, Goldstein M, Vernon I. Galaxy Formation: A Bayesian Uncertainty Analysis. Bayesian Analysis. 2010 Dec;5(4):619-69. doi:10.1214/10-BA524.

54. Saltelli A. Making best use of model evaluations to compute sensitivity indices. Computer Physics Communications. 2002;145(2):280-97. Available from: https://www.sciencedirect.com/science/article/pii/S0010465502002801. doi:https://doi.org/10.1016/S0010-4655(02)00280-1.

55. Sobol IM. Global sensitivity indices for nonlinear mathematical models and their Monte Carlo estimates. Mathematics and Computers in Simulation. 2001;55(1):271-80. The Second IMACS Seminar on Monte Carlo Methods. Available from: https://www.sciencedirect.com/science/article/pii/S0378475400002706. doi:https://doi.org/10.1016/S0378-4754(00)00270-6.

56. Pukelsheim F. The Three Sigma Rule. The American Statistician. 2012 Feb.

57. Andrianakis I, Vernon IR, McCreesh N, McKinley TJ, Oakley JE, Nsubuga RN, et al. Bayesian History Matching of Complex Infectious Disease Models Using Emulation: A Tutorial and a Case Study on HIV in Uganda. PLOS Computational Biology. 2015 Jan;11(1):e1003968. doi:10.1371/journal.pcbi.1003968.

58. Williamson D, Blaker AT, Hampton C, Salter J. Identifying and Removing Structural Biases in Climate Models with History Matching. Climate Dynamics. 2015 Sep;45(5):1299-324. doi:10.1007/s00382-014-2378-z.

59. Pollard D, Chang W, Haran M, Applegate P, DeConto R. Large Ensemble Modeling of the Last Deglacial Retreat of the West Antarctic Ice Sheet: Comparison of Simple and Advanced Statistical Techniques. Geoscientific Model Development. 2016 May;9(5):1697-723. doi:10.5194/gmd-9-1697-2016.

60. Cornford SL, Seroussi H, Asay-Davis XS, Gudmundsson GH, Arthern R, Borstad C, et al. Results of the Third Marine Ice Sheet Model Intercomparison Project (MISMIP+). The Cryosphere. 2020 Jul;14(7):2283-301. doi:10.5194/tc-14-2283-2020.

61. Seroussi H, Nowicki S, Payne AJ, Goelzer H, Lipscomb WH, Abe-Ouchi A, et al. ISMIP6 Antarctica: A Multi-Model Ensemble of the Antarctic Ice Sheet Evolution over the 21st Century. The Cryosphere. 2020 Sep;14(9):3033-70. doi:10.5194/tc-14-3033-2020.

62. Goelzer H, Nowicki S, Payne A, Larour E, Seroussi H, Lipscomb WH, et al. The Future Sea-Level Contribution of the Greenland Ice Sheet: A Multi-Model Ensemble Study of ISMIP6. The Cryosphere. 2020 Sep;14(9):3071-96. doi:10.5194/tc-14-3071-2020.

63. Ritz C, Edwards TL, Durand G, Payne AJ, Peyaud V, Hindmarsh RCA. Potential Sea-Level Rise from Antarctic Ice-Sheet Instability Constrained by Observations. Nature. 2015 Dec;528(7580):115-8. doi:10.1038/nature16147.

64. Edwards TL, Brandon MA, Durand G, Edwards NR, Golledge NR, Holden PB, et al. Revisiting Antarctic Ice Loss Due to Marine Ice-Cliff Instability. Nature. 2019 Feb;566(7742):58-64. doi:10.1038/s41586-019-0901-4.

65. Crawford AJ, Benn DI, Todd J, Åström JA, Bassis JN, Zwinger T. Marine Ice-Cliff Instability Modeling Shows Mixed-Mode Ice-Cliff Failure and Yields Calving Rate Parameterization. Nature Communications. 2021 May;12(1):2701. doi:10.1038/s41467-021-23070-7.

66. Robel AA, Roe GH, Haseloff M. Response of Marine-Terminating Glaciers to Forcing: Time Scales, Sensitivities, Instabilities, and Stochastic Dynamics. Journal of Geophysical Research: Earth Surface. 2018;123(9):2205-27. doi:10.1029/2018JF004709.

67. Sun S, Pattyn F, Simon EG, Albrecht T, Cornford S, Calov R, et al. Antarctic Ice Sheet Response to Sudden and Sustained Ice-Shelf Collapse (ABUMIP). Journal of Glaciology. 2020 Dec;66(260):891-904. doi:10.1017/jog.2020.67.

68. Gowan EJ, Tregoning P, Purcell A, Lea J, Fransner OJ, Noormets R, et al. ICESHEET 1.0: A Program to Produce Paleo-Ice Sheet Reconstructions with Minimal Assumptions. Geoscientific Model Development. 2016 May;9(5):1673-82. doi:10.5194/gmd-9-1673-2016.

69. Gandy N, Gregoire LJ, Ely JC, Cornford SL, Clark CD, Hodgson DM. Collapse of the Last Eurasian Ice Sheet in the North Sea Modulated by Combined Processes of Ice Flow, Surface Melt, and Marine Ice Sheet Instabilities. Journal of Geophysical Research: Earth Surface. 2021 Apr;126(4). doi:10.1029/2020JF005755.

70. Clark CD, Ely JC, Hindmarsh RCA, Bradley S, Ignéczi A, Fabel D, et al. Growth and Retreat of the Last British–Irish Ice Sheet, 31 000 to 15 000 Years Ago: The BRITICE-CHRONO Reconstruction. Boreas. 2022;51(4):699-758. doi:10.1111/bor.12594.

71. Patton H, Hubbard A, Andreassen K, Auriac A, Whitehouse PL, Stroeven AP, et al. Deglaciation of the Eurasian Ice Sheet Complex. Quaternary Science Reviews. 2017 Aug;169:148-72. doi:10.1016/j.quascirev.2017.05.019.

72. Bradley SL, Milne GA, Shennan I, Edwards R. An Improved Glacial Isostatic Adjustment Model for the British Isles: GLACIAL ISOSTATIC ADJUSTMENT MODEL FOR THE BRITISH ISLES. Journal of Quaternary Science. 2011 Jul;26(5):541-52. doi:10.1002/jqs.1481.

73. Letréguilly A, Reeh N, Huybrechts P. The Greenland Ice Sheet through the Last Glacial-Interglacial Cycle. Palaeogeography, Palaeoclimatology, Palaeoecology. 1991 Oct;90(4):385-94. doi:10.1016/S0031-0182(12)80037-X.

74. Sommers AN, Otto-Bliesner BL, Lipscomb WH, Lofverstrom M, Shafer SL, Bartlein PJ, et al. Retreat and Regrowth of the Greenland Ice Sheet During the Last Interglacial as Simulated by the CESM2-CISM2 Coupled Climate–Ice Sheet Model. Paleoceanography and Paleoclimatology. 2021;36(12):e2021PA004272. doi:10.1029/2021PA004272.

75. Hay CC, Morrow E, Kopp RE, Mitrovica JX. Probabilistic Reanalysis of Twentieth-Century Sea-Level Rise. Nature. 2015 Jan;517(7535):481-4. doi:10.1038/nature14093.

76. Zhou Y, McManus J. Extensive Evidence for a Last Interglacial Laurentide Outburst (LILO) Event. Geology. 2022 May;50(8):934-8. doi:10.1130/G49956.1.

77. Creel R, Austermann J, Dyer B. Delayed Laurentide Ice Sheet Melt during the Last Interglacial Causes Sea Level Oscillation Due to Glacial Isostatic Adjustment. In: AGU23. AGU; 2023. .

Fig 4. Relative Sea-Level Dataset. (Top) Map of RSL data locations across northwest Eurasia grouped in 13 regions based upon similar RSL trends. (Bottom) For each region, timeseries of marine limiting (blue, up-arrow marker), terrestrial limiting (green, down-arrow marker) and sea-level index points (orange, round marker) are shown with 1σ uncertainty bounds in age and RSL for absolute dated ages (curved uncertainty) and age range with 1σ RSL uncertainty for relative ages (square uncertainty).

Fig 5. Eurasian Relative Sea-Level Ensemble. Simulated RSL ensemble mean over Eurasia at (A) 122 ka, (B) 118 ka, and corresponding standard deviation at (D) 122 ka and (E) 118 ka. Panels also show the (C) mean and (F) standard deviation of the average rate of RSL change over the LIG.

Fig 6. Regional sensitivities. Map showing each sea-level region (defined in Fig 4) coloured by the magnitude of the relative first-order sensitivity contribution of (A) Antarctic, (B) Eurasian ice-sheet volume, and (C) GIA model parameters. Regional mean values are a result of mean sensitivity indices calculated at each data site.

Fig 7. Relative Sea-Level Model Bias. Maps showing the (A) mean and (B) standard deviation of the estimated model bias field. Data points are coloured with the calculated model bias value.

Fig 8. Optimum input values. Probability density functions of the posterior model input parameter distributions. Distributions are of the closest 10% of simulation, determined via history matching, to RSL data from (blue) all regions and (orange) the subset of regions most sensitive to Antarctica. The dashed grey line shows the probability density functions of the original, prior parameter sample.

Fig 9. Refined Last Interglacial Antarctic Melt Scenarios. Ensemble of LIG AIS melt scenarios before (left, orange) and after (right, blue) history matching against sea-level data in regions sensitive to AIS melt. Plots show the ensemble median (solid line), 66th percentile *likely* (dark shaded region), and 90th percentile *very likely* (light shaded region) ranges of AIS sea-level equivalent volume contribution during the LIG.

Fig 10. Pairwise Implausibility Pattern of East and West Antarctic Melt. Panel showing the pattern of average implausibility for EAIS and WAIS melt across their respective, discretised value ranges. Each pixel represents the average implausibility given fixed values of EAIS and WAIS sea-level contributions over a 1000-member random parameter sample of all other parameters. A darker pixel colour refers to a lower average implausibility value. The simple diagonal gradient pattern indicates that similar implausibility values are observed for similar total melt contributions, regardless of whether they are sourced from EAIS or WAIS.

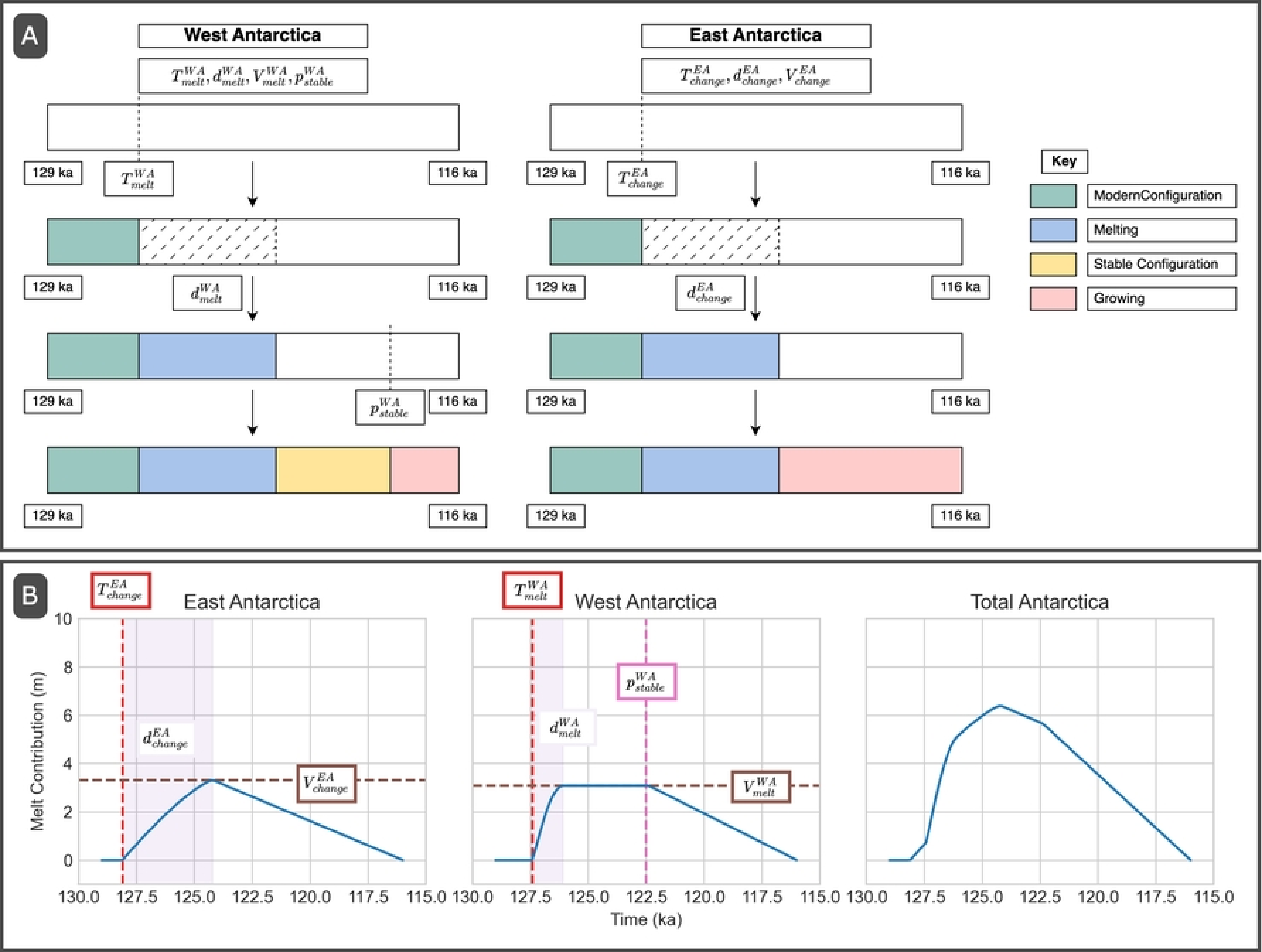
A
West Antarctica
$T^{WA}_{melt}, d^{WA}_{melt}, V^{WA}_{melt}, p^{WA}_{stable}$
129 ka
T^{WA}_{melt}
116 ka
d^{WA}_{melt}
p^{WA}_{stable}
East Antarctica
$T^{EA}_{change}, d^{EA}_{change}, V^{EA}_{change}$
T^{EA}_{change}
d^{EA}_{change}
Key
ModernConfiguration
Melting
Stable Configuration
Growing
B
East Antarctica
West Antarctica
Total Antarctica
T^{EA}_{change}
d^{EA}_{change}
V^{EA}_{change}
T^{WA}_{melt}
d^{WA}_{melt}
p^{WA}_{stable}
V^{WA}_{melt}
Melt Contribution (m)
Time (ka)
10
8
6
4
2
0
130.0
127.5
125.0
122.5
120.0
117.5
115.0

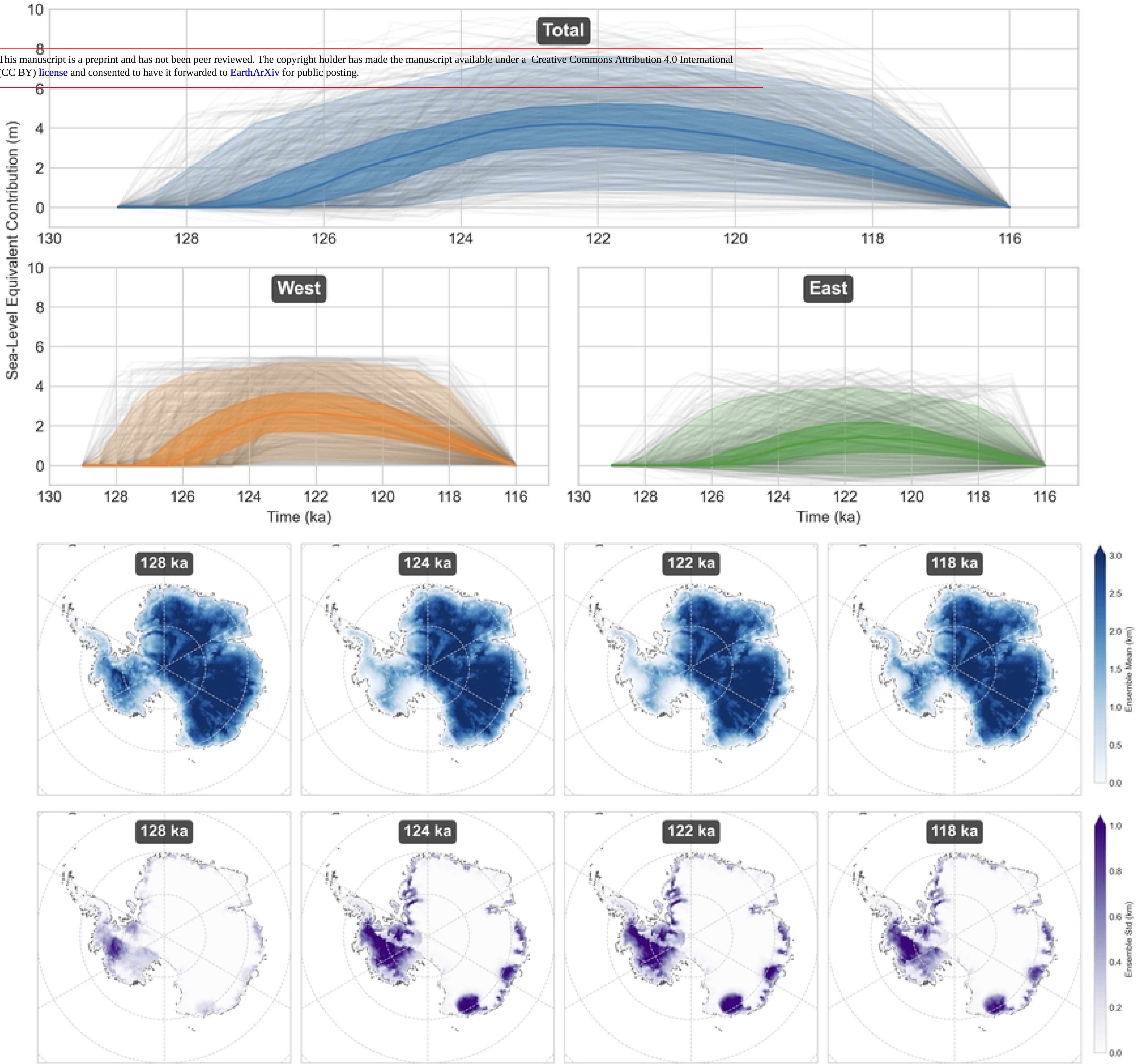
Total
West
East
Sea-Level Equivalent Contribution (m)
Time (ka)
Time (ka)
128 ka
124 ka
122 ka
118 ka
Ensemble Mean (km)
Ensemble Std (km)

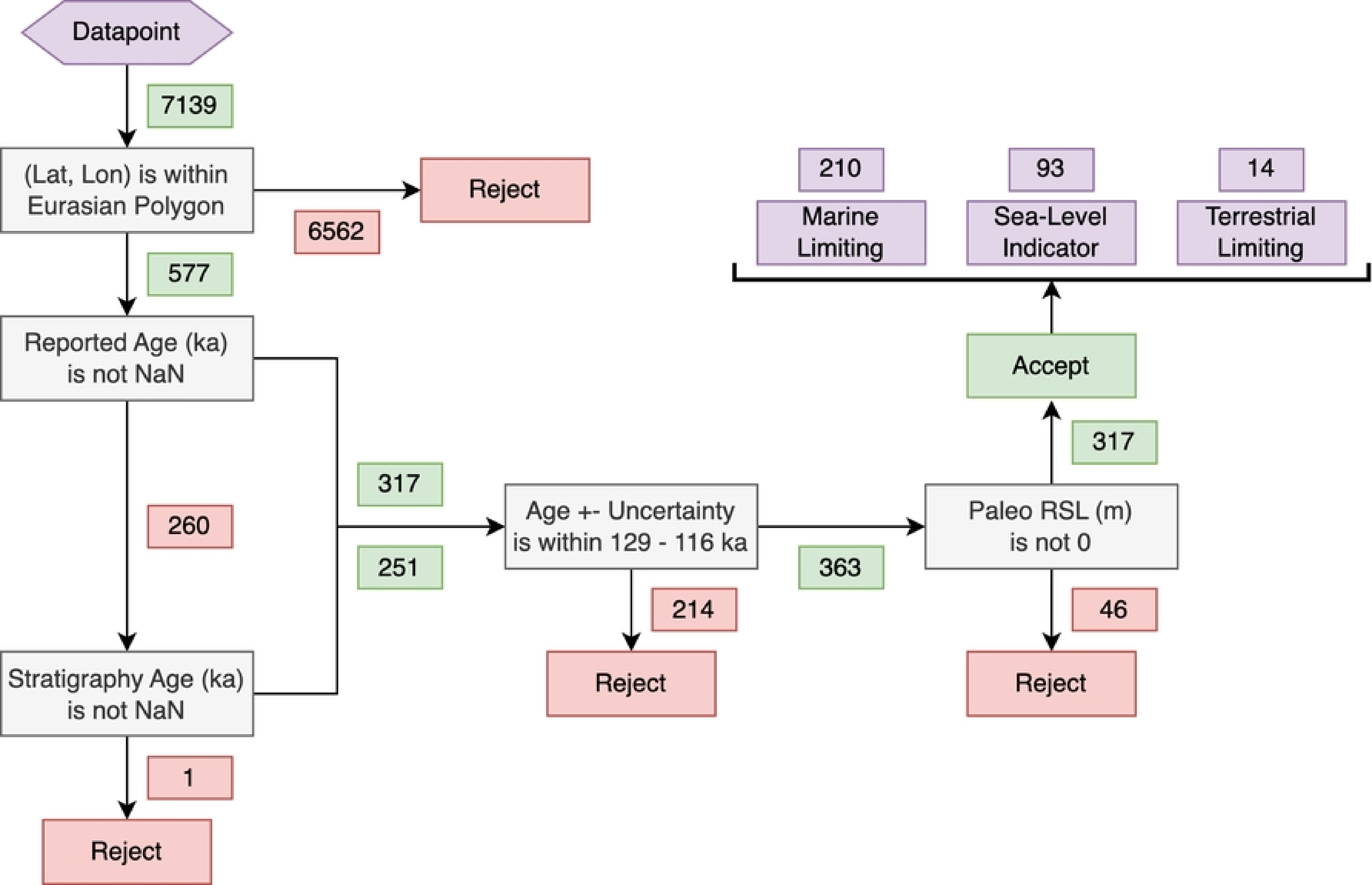
Datapoint
7139
(Lat, Lon) is within Eurasian Polygon
Reject
6562
577
Reported Age (ka) is not NaN
260
317
251
Age +- Uncertainty is within 129 - 116 ka
214
Reject
363
Paleo RSL (m) is not 0
46
Reject
317
Accept
210
Marine Limiting
93
Sea-Level Indicator
14
Terrestrial Limiting
Stratigraphy Age (ka) is not NaN
1
Reject

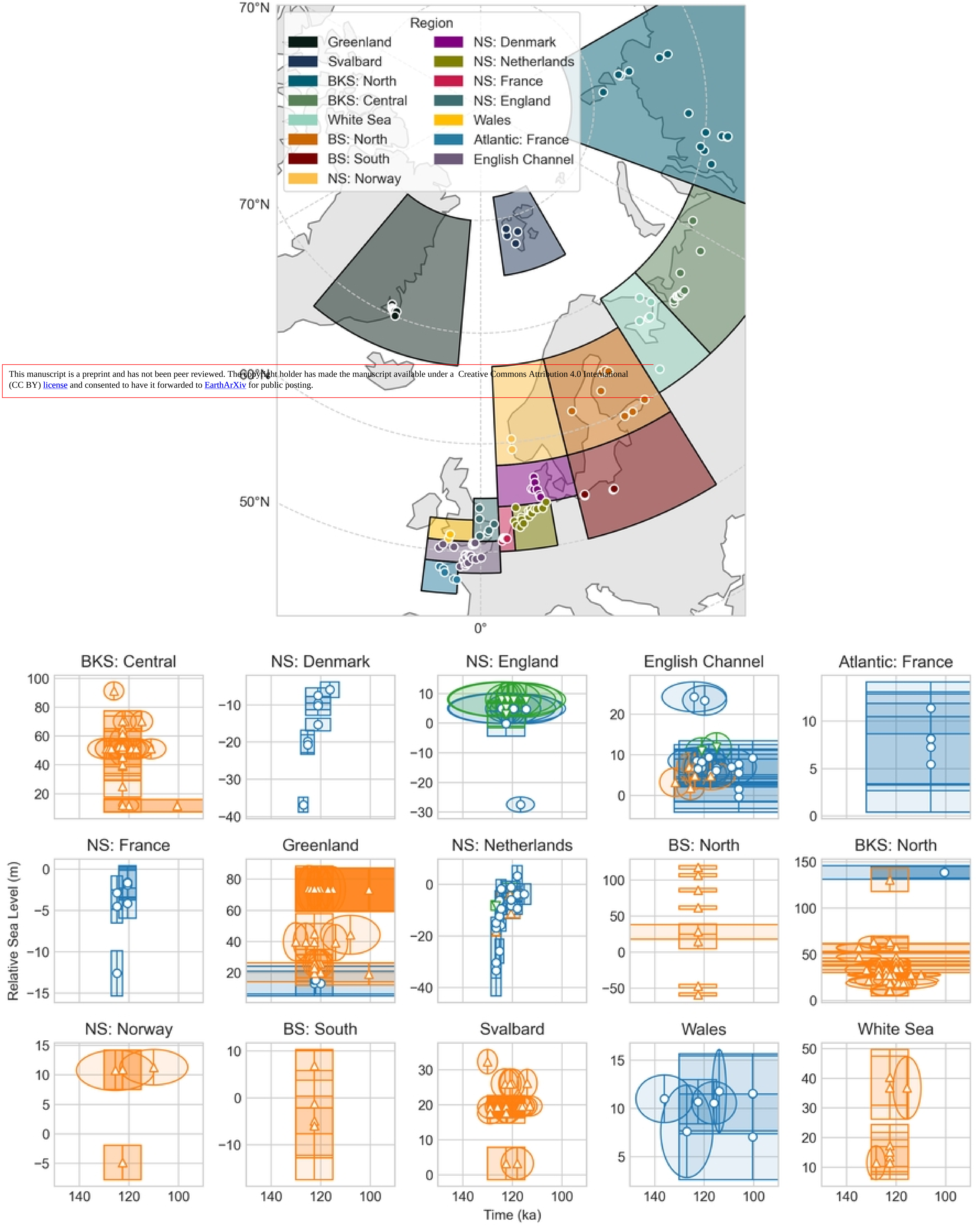

Region
Greenland
Svalbard
BKS: North
BKS: Central
White Sea
BS: North
BS: South
NS: Norway
NS: Denmark
NS: Netherlands
NS: France
NS: England
Wales
Atlantic: France
English Channel
70°N
70°N
60°N
50°N
0°
BKS: Central
NS: Denmark
NS: England
English Channel
Atlantic: France
NS: France
Greenland
NS: Netherlands
BS: North
BKS: North
NS: Norway
BS: South
Svalbard
Wales
White Sea
Relative Sea Level (m)
Time (ka)

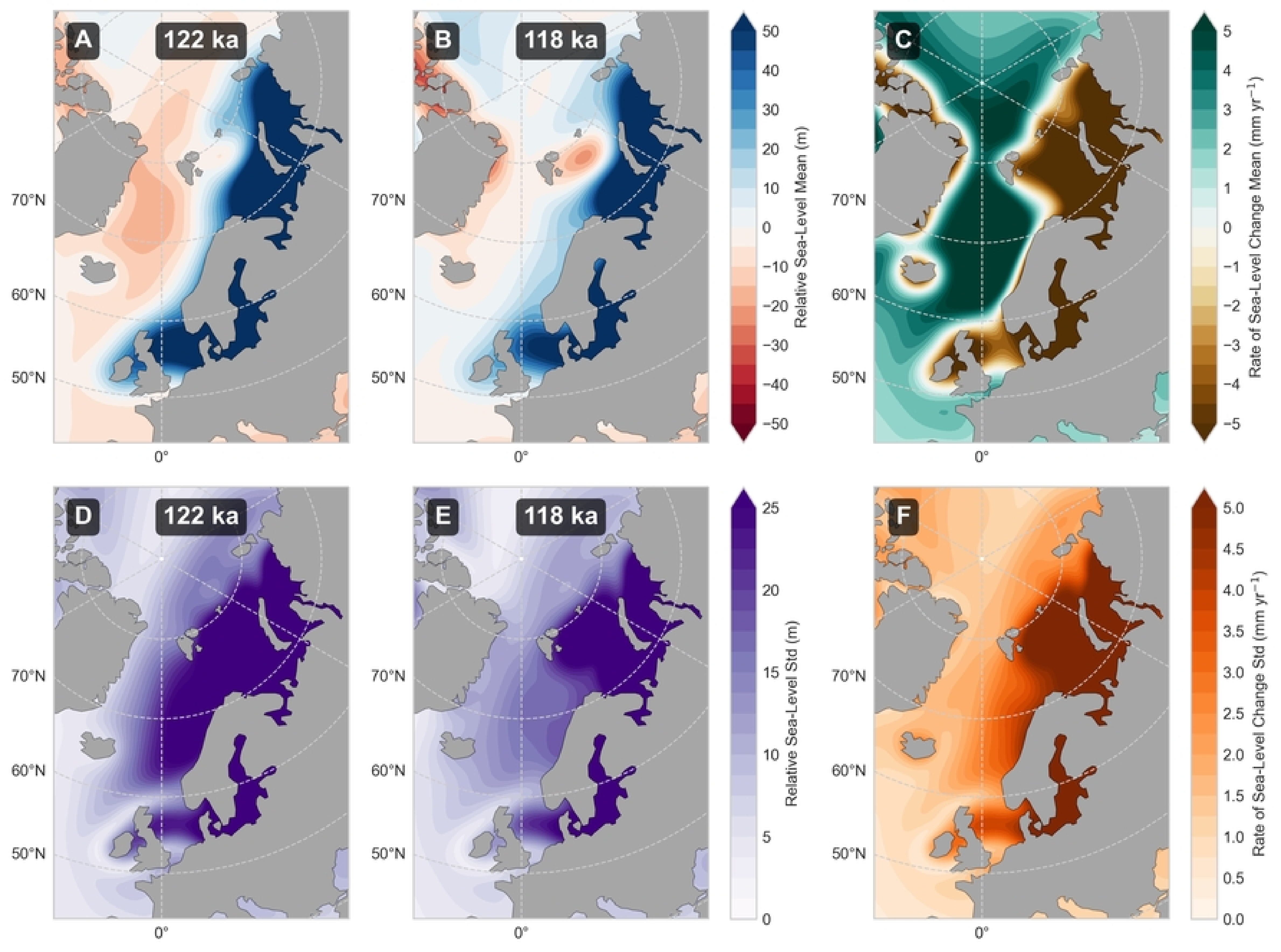
A
122 ka
B
118 ka
C
D
122 ka
E
118 ka
F
70°N
60°N
50°N
0°
Relative Sea-Level Mean (m)
50
40
30
20
10
0
−10
−20
−30
−40
−50
Rate of Sea-Level Change Mean (mm yr−1)
5
4
3
2
1
0
−1
−2
−3
−4
−5
Relative Sea-Level Std (m)
25
20
15
10
5
0
Rate of Sea-Level Change Std (mm yr−1)
5.0
4.5
4.0
3.5
3.0
2.5
2.0
1.5
1.0
0.5
0.0

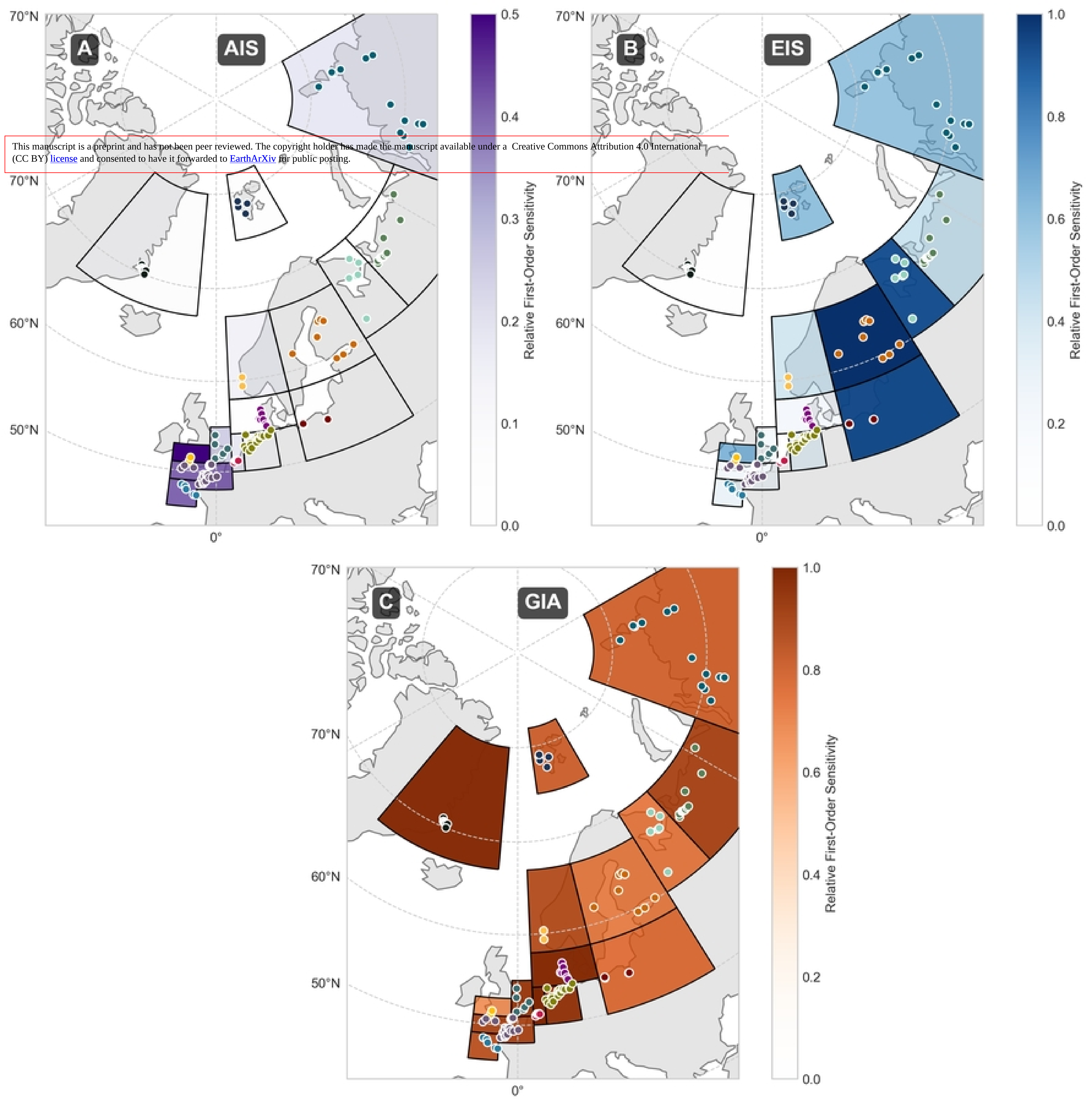
A
AIS
B
EIS
C
GIA
70°N
60°N
50°N
0°
Relative First-Order Sensitivity
0.0
0.1
0.2
0.3
0.4
0.5
0.6
0.8
1.0

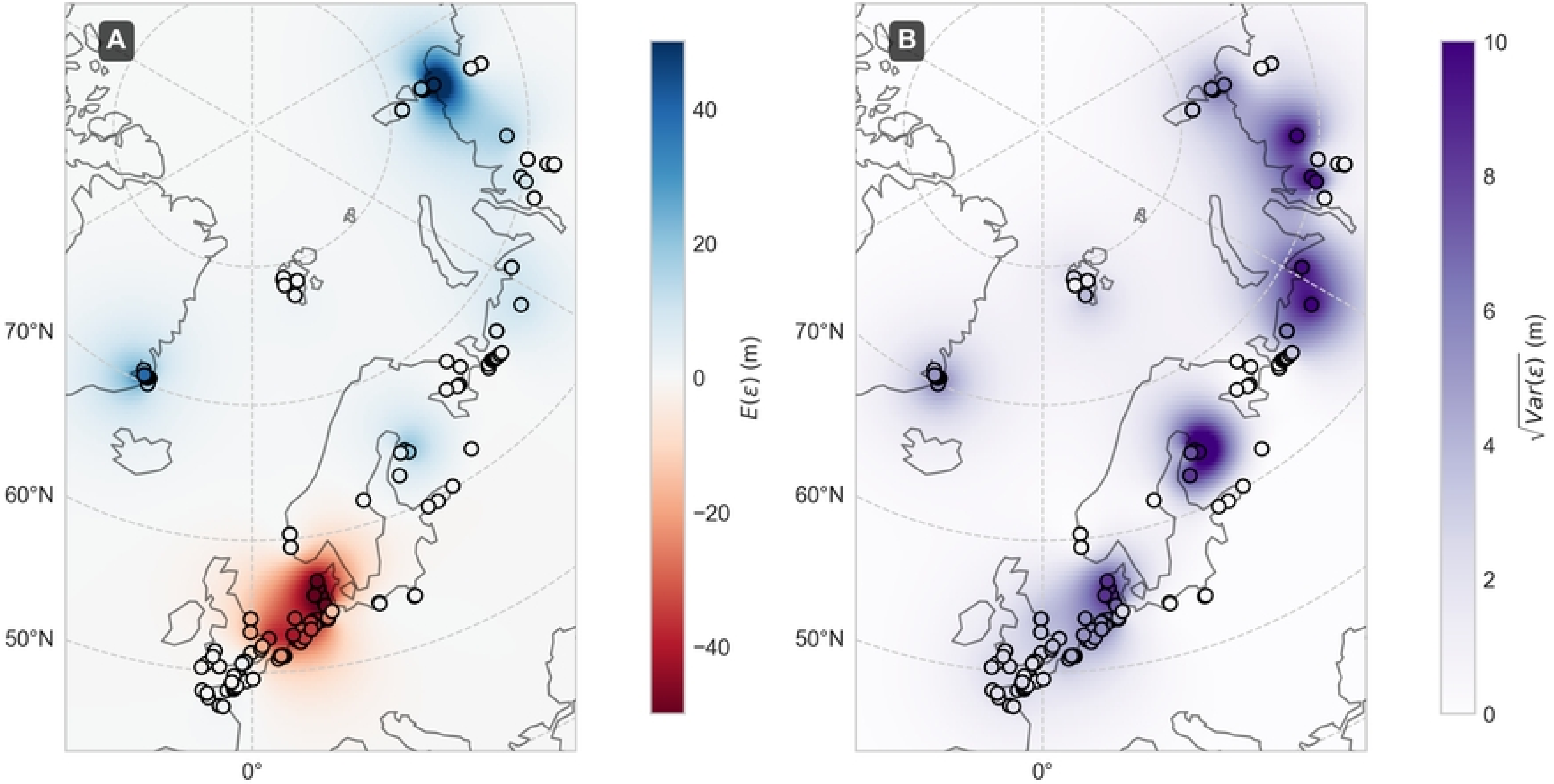
A
B
70°N
60°N
50°N
0°
40
20
0
−20
−40
E(ε) (m)
10
8
6
4
2
0
√Var(ε) (m)

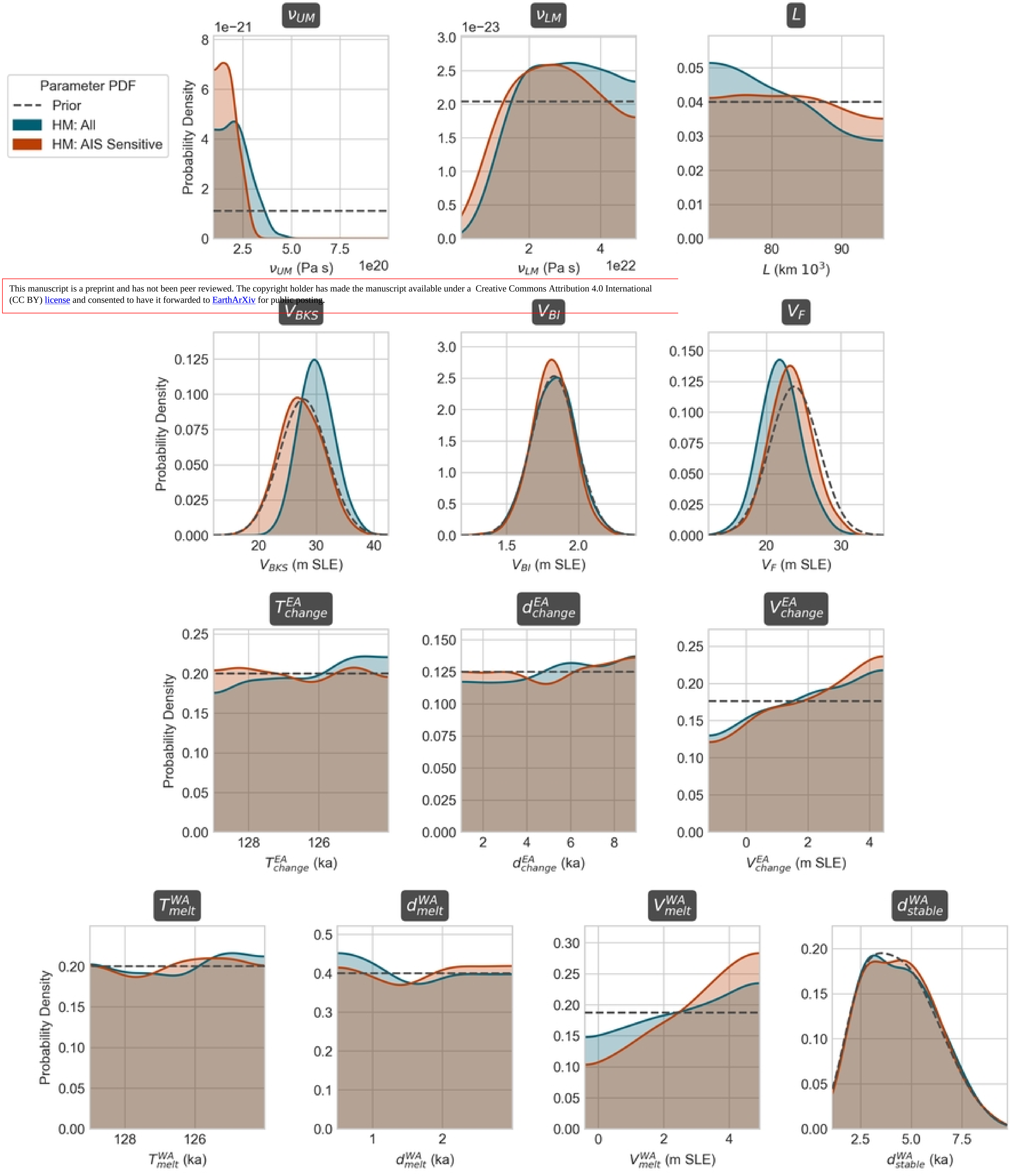

Parameter PDF
Prior
HM: All
HM: AIS Sensitive
ν_{UM}
ν_{LM}
L
V_{BKS}
V_{BI}
V_F
T^{EA}_{change}
d^{EA}_{change}
V^{EA}_{change}
T^{WA}_{melt}
d^{WA}_{melt}
V^{WA}_{melt}
d^{WA}_{stable}
Probability Density
1e−21
1e−23
1e20
1e22
ν_{UM} (Pa s)
ν_{LM} (Pa s)
L (km 10^3)
V_{BKS} (m SLE)
V_{BI} (m SLE)
V_F (m SLE)
T^{EA}_{change} (ka)
d^{EA}_{change} (ka)
V^{EA}_{change} (m SLE)
T^{WA}_{melt} (ka)
d^{WA}_{melt} (ka)
V^{WA}_{melt} (m SLE)
d^{WA}_{stable} (ka)

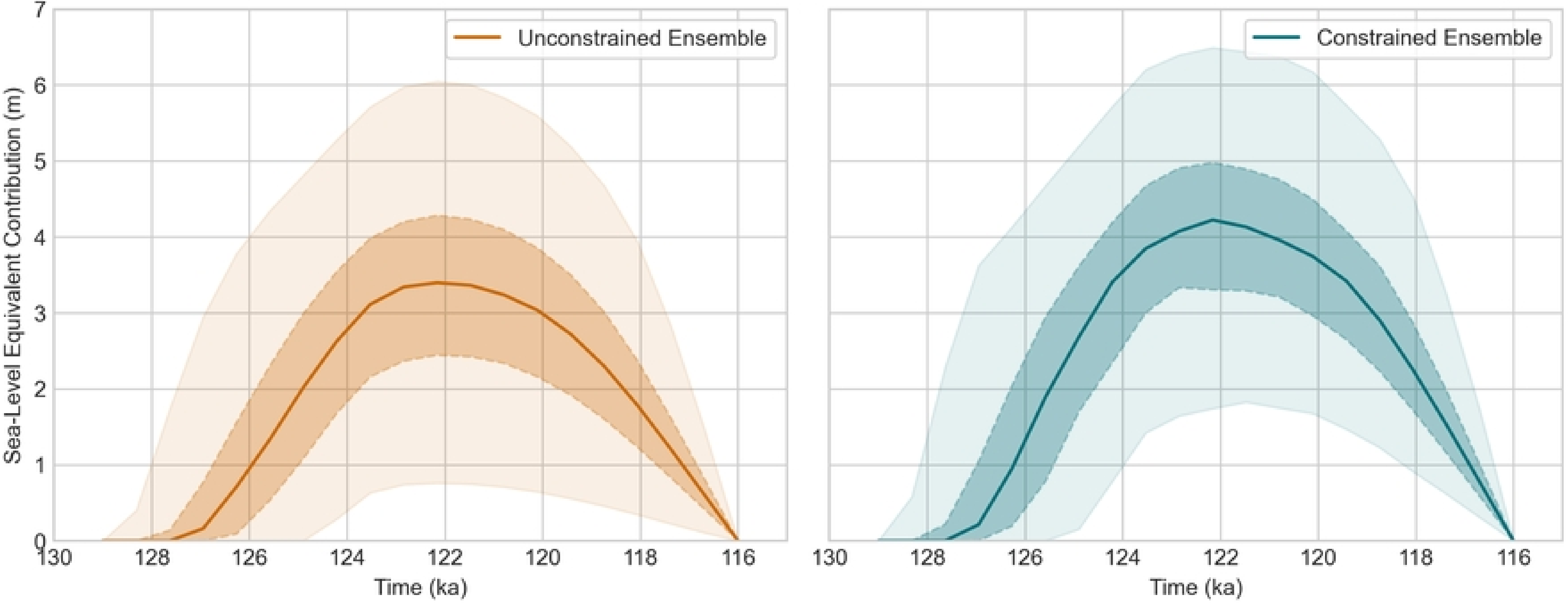

Unconstrained Ensemble
Constrained Ensemble
Sea-Level Equivalent Contribution (m)
0
1
2
3
4
5
6
7
130
128
126
124
122
120
118
116
Time (ka)
Time (ka)

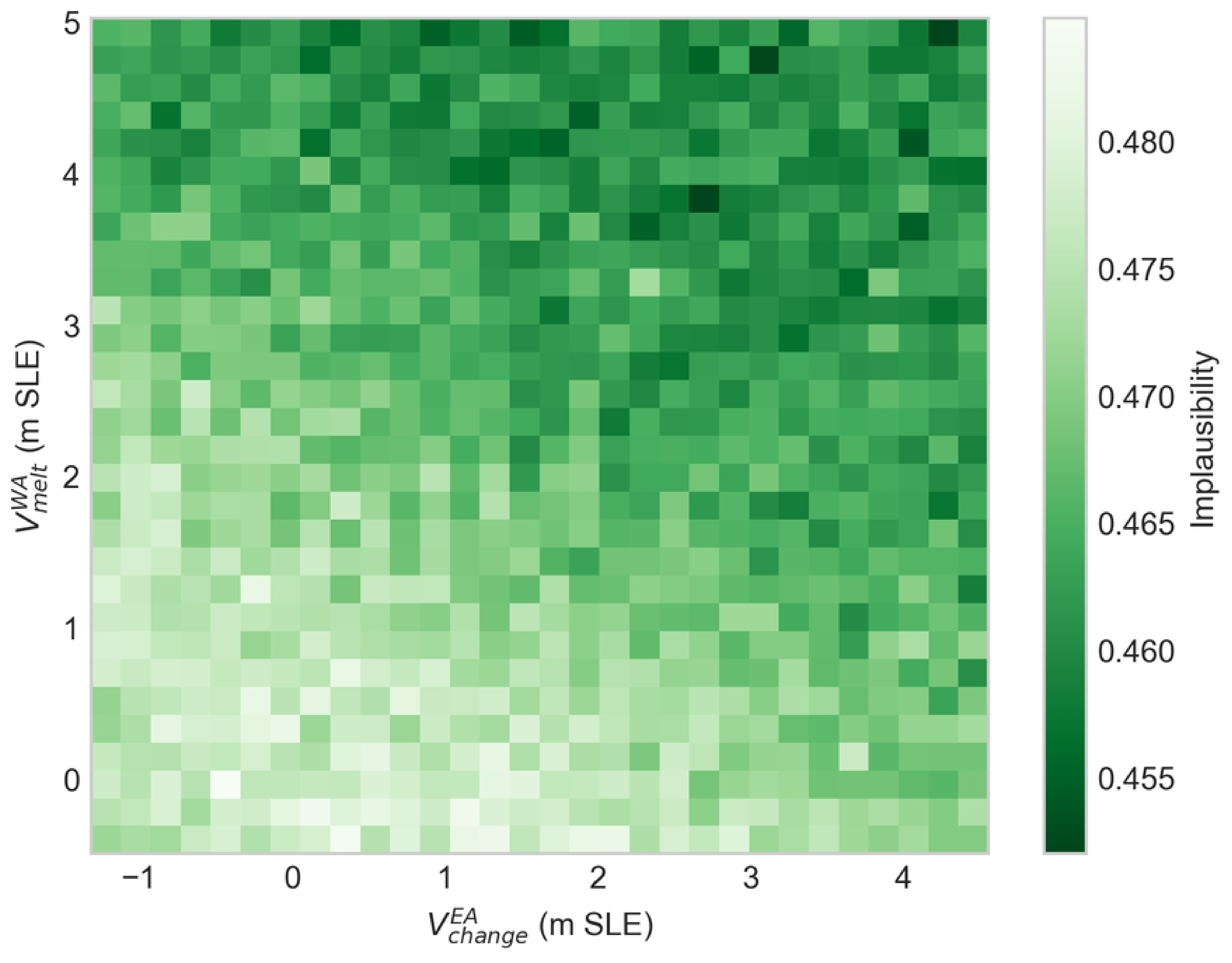

V_{melt}^{WA} (m SLE)
5
4
3
2
1
0
−1
0
1
2
3
4
V_{change}^{EA} (m SLE)
Implausibility
0.480
0.475
0.470
0.465
0.460
0.455